Nanobody-based sensors reveal a high proportion of mGlu heterodimers in the brain

Jiyong Meng, Chanjuan Xu, Pierre-André Lafon, Salomé Roux, Michaël Mathieu, Rui Zhou, Pauline Scholler, Emilie Blanc, Jérôme Becker, Julie Le Merrer, et al.

Nanobody-based sensors reveal a high proportion of mGlu heterodimers in the brain

Jiyong Meng[1,2,3,8], Chanjuan Xu[1,3,8], Pierre-André Lafon[1], Salomé Roux[2], Michaël Mathieu[2], Rui Zhou[1], Pauline Scholler[2], Emilie Blanc[2], Jérôme A. J. Becker[4,5], Julie Le Merrer[4,5], Javier González-Maeso[6], Patrick Chames[7], Jianfeng Liu[1,3,9] Jean-Philippe Pin[2,9] and Philippe Rondard[2,9]

[1] Cellular Signaling Laboratory, International Research Center for Sensory Biology and Technology of MOST, Key Laboratory of Molecular Biophysics of MOE, and College of Life Science and Technology, Huazhong University of Science and Technology, 430074 Wuhan, China.

[2] Institut de Génomique Fonctionnelle, Université de Montpellier, CNRS, INSERM, 34094 Montpellier Cedex 5, France.

[3] Bioland Laboratory, Guangzhou Regenerative Medicine and Health Guangdong Laboratory, 510005 Guangzhou, China.

[4] Physiologie de la Reproduction et des Comportements, INRAE UMR0085, CNRS UMR7247, IFCE, Université de Tours, INSERM, 37380 Nouzilly, France.

[5] UMR1253, iBrain, Université de Tours, INSERM, CNRS, 37200 Tours, France.

[6] Department of Physiology and Biophysics, Virginia Commonwealth University School of Medicine, Richmond, VA 23298, USA.

[7] Institut Paoli-Calmettes, Aix Marseille University, CNRS, INSERM, CRCM, 13009 Marseille, France.

[8] Co-first authors.

[9] To whom correspondence may be addressed. Email: philippe.rondard@igf.cnrs.fr, jean-philippe.pin@igf.cnrs.fr or jfliu@mail.hust.edu.cn.

Keywords:

G protein-coupled receptor | metabotropic glutamate receptor | nanobody | time-resolved FRET | heterodimer | neurotransmitter receptor | neuroreceptor | membrane receptor | olfactory bulb

Abstract

Membrane proteins, including ion channels, receptors and transporters are often composed of multiple subunits and can form large complexes. Their specific composition in native tissues is difficult to determine and remains largely unknown. In this study, we developed a method for determining the subunit composition of endogenous cell surface protein complexes from isolated native tissues. Our method relies on nanobody-based sensors, which enable the proximity detection between subunits in time-resolved FRET measurements. Additionally, given the conformation-specific nanobodies, the activation of these complexes can be recorded in native brain tissue. Applied to the metabotropic glutamate receptors in different brain regions, this approach revealed the clear existence of functional mGlu2-4 heterodimers in addition to mGlu2 and mGlu4 homodimers. Strikingly, the mGlu4 subunits appear to be mainly heterodimers in the brain. Overall, these versatile biosensors can determine the presence and activity of endogenous membrane proteins in native tissues with high fidelity and convenience.

Main Text

Many membrane proteins, including receptors, ion channels, and transporters, are composed of multiple subunits [1-3], and can form oligomers [4]. Auxiliary subunits can also associate with such complexes and affect their overall structure, function, and localization [5]. A major challenge is to investigate these membrane complexes in native conditions without disrupting their environment, since their interactions with lipids and associated proteins could be critical for their assembly and function.

Only a limited number of methods enable the validation of native membrane protein complexes, and are often difficult and time-consuming [6]. They often rely on tissue treatments, membrane fraction preparation, solubilization, or mass spectrometry analysis [6, 7] and chemical cross-linking is sometimes required. Good alternatives are proximity interaction assays that rely on optical detection, but several of these lack spatial resolution (around 40 nm) [8, 9]. It is then difficult to rule out the possibility of proteins not interacting directly [10]. Often, these techniques requires covalent labeling [10], or recombinant fusion proteins.

An attractive approach to examine protein complexes is the use of time-resolved FRET (TR-FRET) [4, 11] (**Fig. 1**). It relies on resonance energy transfer between two fluorophores, with a distance limit of 15 nm between the long-lasting emission donor and acceptor [12], compatible with the size of multi-subunit proteins. A major advantage is the long lifetime of the donor, which enables a delay between its excitation and the measurement of the emission of the sensitized acceptor, strongly reducing the background fluorescence from biological systems. Fluorophores compatible with TR-FRET can be easily attached to antibodies [11], antibody fragments [13] or even small ligands [4] specific to the protein complex under analysis, allowing the analysis of native protein complexes. TR-FRET is thus a highly sensitive technique that is compatible with the detection of endogenous and low-expressed proteins in native tissues [4].

The use of small antibody fragments, such as camelid single-domain antibodies, called V_HH or nanobodies (15 kDa, ~2.5 nm) [14], can result in a high spatial resolution of the protein complexes detected by TR-FRET, higher than with conventional antibodies (~15 nm) [11, 13]. Moreover nanobodies can recognize conformational epitopes, allowing the detection of specific conformations of membrane proteins, such as the active [15-17] or resting state [18, 19]. Nanobodies that potentiate or activate metabotropic glutamate (mGlu) receptors were recently reported [15, 17].

mGlu receptors are G protein-coupled receptors activated by the neurotransmitter glutamate, which tune the activity of many synapses [20]. They are therapeutic targets for several drugs under development for neurological and psychiatric diseases. Eight genes encoding mGluRs have been identified that generate receptors mGlu1 to 8. These are mandatory homodimers with both subunits linked by a disulfide bond, a quaternary structure essential for their activity [21-23]. This is well-illustrated by the latest structures of full-length mGlu dimers in their active and inactive states [24, 25]. These structural studies confirmed a specific symmetrical conformation of the large extracellular glutamate binding domains (ECD), with both domains closed and in a specific active orientation, while the dimer of 7TM domains is asymmetric, with only one capable of G protein activation.

Ten years ago, we reported that these mGlu subunits could also assemble into heterodimers with specific combinations, revealing the possible existence of 16 additional mGlu receptors [26]. Since then, specific pharmacological properties of these heterodimers have been reported, providing indirect evidence of their existence in the brain [27-29]. However, such data could also be explained by functional cross-talk between colocalized homodimeric receptors. In addition, these studies did not reveal the proportion of such heterodimers in the brain compared to homodimers.

In the present study, using specific nanobodies for both mGlu2 and mGlu4 subunits, we were able to reveal the existence of mGlu2-4 heterodimers, in addition to mGlu2 and mGlu4 homodimers, in various brain regions. We also confirm their specific pharmacological properties and reveal that mGlu2-4 is a major type of receptor containing the mGlu4 subunit in the brain outside the cerebellum. These data demonstrate the effectiveness of our approach in deciphering the subunit composition of membrane protein complexes in their native environment and in providing relative quantification of endogenous membrane receptor species in native tissues.

Results

Among the possible 16 mGlu heterodimers observed in recombinant cells [26, 30], the mGlu2-4 heterodimer is the most investigated [27-29], but its existence and abundance in the brain remain unclear. To clarify this issue in different brain areas, we have developed two kinds of nanobody-based TR-FRET sensors (**Fig. 1**): 1) conformational sensors, or "biosensors," that reveal the activation of these receptors upon agonist binding; and 2) the "detectors" that enable the relative quantification of both mGlu homo- and heterodimers.

mGlu2 FRET-based conformational biosensor

We first developed a "biosensor" for the mGlu2 homodimer, by taking advantage of a pair of specific and high affinity nanobodies for the mGlu2 receptor, DN10 and DN1 [15]. DN10 specifically recognizes the receptor dimer in its active state, whereas DN1 is not sensitive to the conformational state (**Fig. 2a**). The DN10 epitope overlaps that of DN13 [15] that is located at an interface of the two ECDs of the mGlu2 homodimer in its active form exclusively [24], the nanobody contacting both subunits. In contrast to DN13, DN10 can also bind to the active mGlu2-4 heterodimer, as shown below, likely because the mGlu4 part of the epitope is compatible with DN10 binding. In contrast, the DN1 epitope remains unknown [15]

(**Supplementary Table 1 and Table 2**). When DN1 and DN10 were covalently labeled with donor Lumi4-Tb and acceptor d2, respectively, a FRET signal was measured in cells expressing mGlu2 in the presence of the mGlu2/3 agonist LY379268, but not with the antagonist LY341495 (**Fig. 2b**). No signal was measured when DN10-d2 was absent (**Extended Data Fig. 1a**), and the FRET signal followed a saturation curve with the increase of DN10-d2 and a fixed concentration of DN1-Tb (**Extended Data Fig. 1b**). The signal was specific to mGlu2, as no signal was measured with other mGluRs (**Extended Data Fig. 1c**). Finally, DN10-Tb and DN1-d2 can also detect endogenous mGlu2 in rat hippocampal neurons by TR-FRET microscopy (**Extended Data Fig. 2**).

This pair of nanobodies could also be used with dissociated cells from different mouse brain regions (**Extended Data Fig. 3a,b**). The more cells, the higher the FRET signal with the nanobodies in the presence of agonists (**Extended Data Fig. 3c**). The slopes, representative of the FRET signal per amount of brain cells, revealed a high signal in the cerebellum and other regions (**Fig. 2c**), consistent with DN1-d2 staining of brain slices (**Extended Data Fig. 4**)[31, 32]. No signal was detected from *Grm2* knockout (*Grm2*$^{-/-}$; called mGlu2 KO in this study) mice (**Fig. 2c, Extended Data Fig. 4**). Altogether, these data validate the use of this pair of nanobodies in the detection of endogenous active mGlu2 receptors.

This conformational biosensor is a sensitive tool to report the rearrangement of the mGlu2 ECD upon agonist activation. In transfected cells, the TR-FRET signal generated using increasing concentrations of various full and partial agonists revealed potencies and efficacies consistent with SNAP-tag FRET based assay[33, 34] (**Fig. 2d**). The potencies also correlated well with those measured by the accumulation of inositol phosphate-1 (IP_1) (**Fig. 2e,f**). Such a good correlation between the potencies of partial and full agonists observed in both assays was not expected, as the amplification resulting from receptor reserve is expected to increase more the potencies of full agonists than those of partial agonists. The good correlation may be due to the

fact that the efficacy of partial agonists is closer to a full efficacy in the presence of the G protein bound to the active receptor [33, 35]. Taken together, these data show that this nanobody-based biosensor constitutes a new generation of untagged mGlu conformational sensors.

This biosensor can also reveal the activation of endogenous mGlu2 receptors in dissociated cells from various brain regions. The agonist-induced change in FRET observed in the cortex, hippocampus, and cerebellum was similar to that found with transfected cells (**Fig. 2g–i**). The antagonist LY341495 was also found to inhibit both the basal signal likely generated by ambient glutamate in the assay, and the agonist at it EC_{80}.

Altogether, our data demonstrate that this optical nanobody-based biosensor can be used to reveal the activation of endogenous mGlu2 receptors in native dissociated tissues. It represents an innovative assay for throughput screening of the efficacy of drugs on native mGlu2Rs in brain tissue.

Quantification of the mGlu2 homodimer

We next aimed at quantifying of mGlu2 homodimers using DN1-Tb and DN1-d2 as TR-FRET pair, first on the surface of transfected cells (**Fig. 3a**). As expected, this "detector" signal is independent of the conformation of the homodimer, whether bound to an agonist or an antagonist (**Fig. 3b**). The concentrations of the nanobodies were optimized to have a FRET signal proportional to the quantity of mGlu2 over a wide range of receptor amounts (**Extended Data Fig. 5a–c**). This "detector" was also specific for the mGlu2 among all mGlu homodimers (**Fig. 3c**). We also believe that the FRET signal was mostly due to the mGlu2 homodimer, and not higher order oligomers. First, the FRET signal between the DN1 nanobodies was proportional to the number of SNAP-mGlu2 subunits on the cell surface over a wide range of receptor amounts (**Extended Data Fig. 5c**). Second, this linearity was also observed with the "controlled" mGlu2 homodimer formed by the $mGlu2_{C1}$ and $mGlu2_{C2}$ subunits, as previously

described [26, 36] (**Extended Data Fig. 5d**). In these constructs, the C-terminal of the mGlu2 subunits was replaced by that of the modified $GABA_{B1}$ (C1) or $GABA_{B2}$ (C2) subunits, respectively, preventing any of these to reach the cell surface alone. Indeed, only C1-C2 dimers can reach the cell surface [26]. However, when using a similar controlled mGlu2-4 heterodimer made of $mGlu2_{C1}$ and $mGlu4_{C2}$ subunits, no FRET signal with the DN1 "detector" was measured (**Extended Data Fig. 5d**). Under these conditions, the mGlu2-4 heterodimer is present at the cell surface in the absence of both mGlu2 and mGlu4 homodimers. This is consistent with our previous demonstration that the controlled mGlu2-4 heterodimer [26] as well as the mGlu2 homodimer [26, 37, 38] do not have the tendency to form oligomers in transfected cells. Third, the highest FRET signal measured for equal concentrations of donor (DN1-Tb) and acceptor (DN1-d2) was also consistent with the presence of strict mGlu2 homodimers (**Extended Data Fig. 5b**).

By comparing the mGlu2 homodimer "detector" signal in different brain areas (**Fig. 3g** and **Extended Data Fig. 5e**), mGlu2 was found more abundant in the cerebellum (**Fig. 3g**). As a control, no signal was observed in the cerebellum of mGlu2 KO mice. However, this "detector" appears less sensitive than the "biosensor", but this was expected for two main reasons. First, only half of the mGlu2 homodimers can be labeled with two FRET compatible DN1 nanobodies (DN1-Tb and DN1-d2). In contrast, each mGlu2 subunit will be labeled with two FRET compatible nanobodies in the biosensor assay, DN1-Tb and DN10-d2, such that each mGlu2 homodimers carry two pairs of FRET compatible nanobodies. Second, this biosensor assay detects any active form of the mGlu2 subunits, whether in a homo or heterodimer, in contrast to the "detector" that reveals mGlu2 homodimers only.

Quantification of the mGlu4 homodimer

To quantify the mGlu4 homodimer, we isolated and characterized the nanobody DN42, highly specific for mGlu4 (**Extended Data Fig. 6a,b**). For this study, we used the Fc-DN42 dimeric

construct (80 kDa) as the DN42 monomer has a low affinity after labeling with a fluorophore (~100 nM) that is not compatible with its use with native tissues. Interestingly, Fc-DN42 has a sub-nanomolar affinity for the mGlu4 ECD, and a similar affinity for the inactive and active conformations (**Supplementary Table 1 and Table 2**; **Extended Data Fig. 6c**). We verified by immunofluorescence that Fc-DN42 was able to specifically detect mGlu4 subunits in brain slices of wild-type mice but not in *Grm4* knockout (*Grm4*$^{-/-}$; called mGlu4 KO in this study) mice (**Extended Data Fig. 6d**).

We used Fc-DN42, from now on referred to as DN42, as a "detector" to quantify mGlu4 homodimers, similarly to what was done with DN1 for the mGlu2 homodimers. With optimized concentrations of DN42 (**Extended Data Fig. 7a,b**), a strong FRET signal was measured between DN42-Tb and DN42-d2 in mGlu4 transfected cells specifically (**Fig. 3d-f**), independent from the state of the receptor. As observed with mGlu2, the FRET signal appeared mostly owing to the mGlu4 homodimer, and not to higher order oligomers. First, the signal was proportional to the number of SNAP-mGlu4 subunits on the cell surface over a wide range of receptor amounts (**Extended Data Fig. 7c**). Second, this linearity was also observed with a controlled mGlu4 homodimer, where the C-terminal of mGlu4 subunits was replaced by that of the $GABA_B$ receptor (**Extended Data Fig. 7d**). Lastly, the low FRET signal between mGlu4 subunits measured with the controlled mGlu2-4 heterodimer (**Extended Data Fig. 7d**) may be due to random proximity between these heterodimers, although one cannot exclude a very few mGlu2-4 oligomers. This is also consistent with several reports showing the low probability of mGlu dimers to oligomerize under basal condition[26, 37].

In native brain tissues, this pair of labeled DN42 nanobodies revealed a detectable signal mainly in the cerebellum of the wild-type and mGlu2 KO mice, but not in mGlu4 KO mice (**Fig. 3h** and **Extended Data Fig. 7e**). Significant signal could also be observed in the prefrontal cortex (PFC) (**Figure 3h, inset**), but the signals measured in other brain areas were

not significant indicating that our assay is not sensitive enough to detect mGlu4 homodimers in these areas, if any. This agrees with the strong expression of mGlu4 in the cerebellum [31], as shown also by DN42-stained brain slides, especially in the molecular layer (**Extended Data Fig. 6d**). Altogether, our results show a very low expression of the mGlu4 homodimer in most brain regions except for the cerebellum, not really consistent with the immunostaining data [31] (**Extended Data Fig. 6d**), suggesting that mGlu4 subunits could be associated with other mGlu subunits outside the cerebellum.

An mGlu2-4 heteromer FRET-based detector

Recent studies argue in favor of the existence of endogenous mGlu2-4 receptors in neuronal cell lines [27], as well as in the PFC, striatum and hippocampus [27-29] as suggested by electrophysiological, pharmacological and biochemical data. Although convincing, the results provide indirect evidence of the endogenous mGlu2-4 heterodimer [27-29]. More direct evidence for this heterodimer could come from a proximity assay based on FRET between the mGlu2 and mGlu4 subunits in tissues, owing to the nanobodies described above.

Thus, we used DN1 and DN42 nanobodies to detect mGlu2-4 heterodimers first on transfected cells. Using the optimized concentrations of DN1 and DN42 (**Supplementary Table 1**, **Extended Data Fig. 8a,b**), a strong FRET signal was measured, proportional to the amount of controlled mGlu2-4 heterodimers on the cell surface (**Extended Data Fig. 8c**). We also showed that the FRET signal could not result from mGlu homodimers (**Extended Data Fig. 8d**). Because mGlu2-4 is likely co-expressed with mGlu2 and mGlu4 homodimers in native tissues, we used two methods to detect mGlu2-4 heterodimers in transfected cells. First, we used cells co-expressing $mGlu2_{C1}$ and $mGlu4_{C2}$ (**Extended Data Fig. 5d and 7d**) such that only heterodimers could reach the surface (**Fig. 4a**). Second, the wild-type mGlu subunits were co-transfected to obtain a mix of mGlu2 and mGlu4 homodimers together with the mGlu2-4 heterodimer on the cell surface (**Fig. 4b**) [26, 27]. In both cases, a strong FRET signal was

measured whether the receptors were activated with the mGlu2 agonist LY379268 or antagonized with LY341495 (**Fig. 4c,d**).

Applied to isolated brain cells, this nanobody FRET pair generated a strong signal in the olfactory bulb (OB), PFC, striatum and hippocampus (**Fig. 4e** and **Extended Data Fig. 8e**) where mGlu2 (**Fig. 3g**) but not mGlu4 (**Fig. 3h**) homodimers have been previously detected. As a control, no signal was measured in the OB from mGlu2 KO or mGlu4 KO mice (**Fig. 4f** and **Extended Data Fig. 8g**). In agreement with these results, co-immunoprecipitation experiments with the OB using DN42 revealed the presence of endogenous mGlu2 in the same complexes as mGlu4 (**Extended Data Fig. 8f**). Notably, the cerebellum did not produce a specific signal between DN1 and DN42 (**Fig. 4e, g**), consistent with mGlu2 and mGlu4 subunits being expressed in different cell types [31, 39, 40] (**Extended Data Fig. 4** and **Extended Data Fig. 6d**). Surprisingly, the slope for the cerebellum was even negative (**Fig. 3e, g** and **Extended Data Fig. 8e,g**), most probably due to the relatively high amount of mGlu4 homodimers in this region that is sufficient to titrate the DN42 present at 1.6 nM in the assay, then resulting in a slight but significant decrease in FRET. In agreement with this hypothesis, the slope was no longer negative for samples from mGlu4 KO mice, whereas it remained negative in samples from mGlu2 KO mice (**Extended Data Fig. 8e, g**).

mGlu2-4 heterodimer FRET-based biosensor

Although the above data provide strong evidence for the presence of mGlu2-4 heterodimers in various brain regions, one cannot exclude that the signal come from the proximity between mGlu2 and mGlu4 homodimers. To bring further evidence of the existence of the endogenous mGlu2-4 heterodimer, we developed a nanobody-based FRET conformational sensor for this heterodimer using DN10 and DN42, as DN10 can bind to the mGlu2-4 heterodimer in the active state only (**Extended Data Fig. 9a,b**; **Supplementary Table 1 and Table 2**). Of note, L-AP4, a partial agonist of the mGlu2-4 heterodimer [17, 27], remains partial in promoting DN10

binding (**Extended Data Fig. 9a,b**), as monitored by the FRET between the nanobody and the SNAP-mGlu4 subunits. Interestingly, DN10 binding to mGlu2-4 in the presence of the mGlu4 agonist L-AP4 (**Extended Data Fig. 9a,c**) was strongly potentiated by the mGlu2 agonist LY379268 (**Extended Data Fig. 9c,e**), whereas L-AP4 did not induce binding of DN10 to the control mGlu2 homodimer (**Extended Data Fig. 9d**).

By combining DN42 that specifically binds to the mGlu4 subunit, and DN10, which binds to the active form of mGlu2-4, we could detect mGlu2-4 activation by FRET (**Fig. 5a–f**, **Extended Data Fig. 9f**), a signal that could not result from either homodimers (**Extended Data Fig. 9g**). Similar data were obtained in cells expressing the controlled mGlu2-4 (**Fig. 5a-c**) and in cells expressing both mGlu2 and mGlu4 subunits (**Fig. 5d-f**). Under the latter conditions, both homodimers were present on the cell surface along with the heterodimer (**Fig. 5d**), demonstrating that they do not interfere with the specific signal generated by the active heterodimer. Under these conditions, the agonist LY379268 generated a large signal that is largely inhibited by the antagonist LY341495 while L-AP4 generated a smaller signal (**Fig. 5b, d,e**). Moreover, as previously reported[17, 27, 34], a strong positive cooperativity was observed between the mGlu2 and the mGlu4 agonists on the heterodimer, illustrated here with the large increase in L-AP4 potency by a low concentration of LY379268 (**Fig. 5c,f** and **Extended Data Fig. 10d**). These data are also consistent with the IP_1 production data obtained in cells expressing controlled mGlu2-4, or both mGlu2 and mGlu4 (**Extended Data Fig. 10a–c**). Altogether, these results show that DN10 and DN42 can be used to detect the active form of the mGlu2-4 heterodimer.

This mGlu2-4 biosensor also detected the activation of endogenous mGlu2-4 heterodimer in dissociated brain cells as revealed by the synergy between the mGlu2 and mGlu4 agonists. The activation of the endogenous mGlu2-4 was revealed by the large FRET signal induced by LY379268 in all regions where the mGlu2-4 heterodimer was detected – i.e.

the OB, PFC, striatum and hippocampus-, but not in the cerebellum (**Fig. 5g**). As expected, the LY379268 effect disappeared in the mGlu4 KO brain samples. In addition, in the OB **(Fig. 5h)**, L-AP4 potency was increased by a low concentration of LY379268 (**Fig. 5i** and **Extended Data Fig. 10e**), as observed in transfected cells. Finally, a nice correlation in agonist potencies measured in transfected cells and in brain samples was observed (**Extended Data Fig. 10f and Extended Data Table 3**). Altogether these results bring further direct evidence for the existence of the mGlu2-4 heterodimer in different brain regions.

mGlu2-4 heterodimer brain distribution

Intriguingly, we detected higher signals using the mGlu2-4 "detector" (**Fig. 4e**), than the mGlu4 homodimer "detector" (**Fig. 3h**) in most brain areas outside the cerebellum. Such a difference in signal intensity was not due to a difference in FRET efficacy between the nanobodies per dimeric combination. This is best illustrated by the perfect correlation between the FRET obtained with either the mGlu4 specific homodimer DN42 "detector," or the mGlu2-4 specific heterodimer DN1-DN42 "detector," relative to the cell surface expression of the SNAP or CLIP subunits **(Fig. 6a)**. These data indicate that there are more mGlu2-4 heterodimers than mGlu4 homodimers in most regions outside the cerebellum (**Fig. 6b**).

Discussion

Our study describes an innovative and general method for the quantification and analysis of endogenous multi-subunit membrane proteins using nanobody-based optical sensors. Using this method, we provide direct evidence for the existence of mGlu2-4 heterodimers in different brain areas. Surprisingly, our results revealed that most mGlu4 subunits are likely associated with another subunit, such as mGlu2, in most brain regions outside the cerebellum.

Our method combines the high spatial resolution of the TR-FRET technology (< 15 nm) with the small size of single-domain nanobodies (~ 2.5 nm) to detect low amounts of

endogenous subunits in native tissues. Obtaining such information in native membranes is essential, as lipid composition and ions likely play an important role in stabilizing protein complexes [41]. No chemical fixation or biochemical treatments of the biological sample are required, in contrast to other analyses, thus preventing the conformational changes of the complex. In addition, our results prove that nanobodies have great potential as TR-FRET probes, which help to solve the shortcomings of small molecules in terms of specificity, which limits their use in TR-FRET experiments [4]. Nanobodies have hydrophilic properties, in contrast to small molecules that can be hydrophobic, and help overcome the limitations of classical antibodies in recognizing specific protein conformations. Nanobodies are small antibodies (ten times smaller than IgGs), easy to engineer, and display good and rapid tissue penetrance [42]. They often recognize conformational and cryptic epitopes, not accessible to classical antibodies. Our method can be applied to any cell surface proteins, including ligand-gated ion channels or transporters [5]. In addition, our method is versatile as the fluorophores can be covalently attached to small ligands, antibody fragments or common antibodies. Finally, our method does not require a high level of expertise or expensive equipment. It only entails working in microplates with standard biochemical protocols and a standard commercial TR-FRET reader. However, the TR-FRET approach may not be appropriate for the detection of heterodimers using microscopy in brain slices, due to the low quantum yield of the donor and the need for a special equipment for the time delay between the excitation and the measurement of the emission signal[43]. It can however be used on cultured neurons **(Extended Data Figure 2).** However, the use of fluorophores compatible with conventional FRET microscopy may allow the detection of dimers in neuronal sub-compartments using microscopy in cultured neurons with a better precision.

Our approach has two major advantages in investigating the endogenous mGlu heterodimers [27-29, 44]. First, it analyzes the heterodimer entity directly and not its downstream

signaling that could result from cross-talk between signaling pathways [45]. Second, our biosensors are good reporters of the conformational change of the receptor during activation, as other sensors of the mGlu receptors [27, 33, 34]. However, whether this approach can be used to detect mGluR activation in real time remains to be tested. For this, the use of fluorophores compatible with conventional FRET measurement will be necessary. It will also be essential to take into consideration the ON rate of binding of the nanobody that recognizes the active form of the receptor, as this may be much slower than the ON rate of mGluR activation that occurs in the sub-millisecond time scale[35, 46]. It is clear that this second point will generate limitations for such analysis. Finally, the pharmacological signature of our new sensors using orthosteric ligands could be defined in transfected cells, and could then be observed in native brain samples.

Our study reveals an intriguing distribution of mGlu4 homodimers, mainly found in the cerebellum, where they do not form detectable heterodimers with mGlu2 as expected as these two subunits are expressed in different types of neurons in the cerebellum. These data appear as an excellent control for our assay. The absence of significant detection of mGlu4 homodimer in most brain regions does not exclude that some homodimers may be present. Indeed, mGlu4 homodimers were proposed at hippocampal-mPFC and amygdala-mPFC synapses [28], and at corticostriatal synapses [29] suggesting that our approach is not sensitive enough to detect those homodimers. However, this conclusion was based on the use of mGlu4 PAMs inactive at mGlu2-4 such as *N*-phenyl-7-(hydroxyimino)cyclopropa[b] chromen-1a-carboxamide (PHCCC). Since the effect of these compounds on mGlu4-3, 4-7 or 4-8 heterodimers[26, 30] is not known, further pharmacological studies on these heterodimers will be necessary to clarify this issue. Whatever, our data clearly show that in many brain regions, there are more mGlu2-4 than mGlu4-4, as a larger signal could be detected with the mGlu2-4 detector, despite a very similar FRET efficacy per dimer. Interestingly, an astonishing distribution of the mGlu2-4

heterodimer was observed, with a high expression in the OB and PFC, in agreement with the demonstration of mGlu2-4 at thalamo-mPFC synapses [28], where they would coexist with mGlu2 homodimers, without excluding low amounts of mGlu4 homodimers. This is consistent with the link between the mGlu2 subunit and psychiatric diseases involving the PFC [47].

Future studies on the existence of other mGlu heterodimers are crucial for assessing the physiological role of the mGlu receptors in the brain, potential new drug targets. Indeed, mGlu4 heterodimers could explain the effect of an mGlu4 allosteric modulator acting in the basal ganglia [48] whereas it has no effect on the mGlu4 homodimer [29]. In addition, mGlu7 heterodimers could also contribute to the enigmatic function of the mGlu7 subunit due to its very low glutamate potency [49], and the effect of mGlu7 negative allosteric modulators with a context-dependent activity [50]. Further studies are necessary to clarify these issues, as well as the functional role and therapeutic potential of these mGlu heterodimers, a step that will require the development of specific ligands for these receptor species.

In conclusion, we have reported a general and versatile approach compatible with the quantification and functional analysis of membrane proteins from endogenous native tissues, without disrupting the membrane environment, but the availability of specific ligands is a major limitation. However, the number of antibodies targeting these proteins, including nanobodies, is rapidly expanding, even those selective of a conformational state [13, 16, 18].

Acknowledgments

We wish to thank Damien Nevoltris and Damien Meyer (IRCM, Marseille, France) for the screening of the nanobodies, and preparing the Fc-DN42 construct, respectively. We thank the Arpège platform of the Institut de Génomique Fonctionnelle for providing facilities and

technical support, the imaging facility Montpellier Ressources Imagerie (MRI), member of the national infrastructure France-BioImaging supported by the French National Research Agency (ANR-10-INBS-04, Investments for the Future), the animal facility RAM-iExplore from BioCampus (Montpellier, France) and Perkin Elmer Cisbio for providing reagents. We thank Cyril Goudet and Thierry Durroux (IGF, Montpellier, France) for providing the mGlu4 KO mice and for the assistance in the TR-FRET microscopy, respectively. J.M. and C.X. were supported by Sino-French Cai Yuanpei program (grant number 201604490217 and 201304490188, respectively). P. R. and J.-P. P. were supported by the Centre National de la Recherche Scientifique (CNRS, PICS n°07030, PRC n°1403), the Institut National de la Santé et de la Recherche Médicale (INSERM, IRP BrainSignal), the Fondation pour la Recherche Médicale (FRM) (Equipe DEQ20170336747), the Eidos collaborative laboratory with Perkin Elmer Cisbio, the Franco-Chinese Joint Scientific and Technological Commission (CoMix) from the French Embassy in China and the LabEx MAbImprove (Grant NR-10-LABX-5301). P.R. and J.-P. P. were supported by the ANR (Grant ANR-15-CE18-0020-01, ANR-20-CE18-0011-01 and ANR-20-CE44-0006-02). J. L. was supported by the Program of Bioland Laboratory (Guangzhou Regenerative Medicine and Health Guangdong Laboratory; grant number 2010A080813001), the Ministry of Science and Technology of China (grant number 2018YFA0507003), the National Natural Science Foundation of China (NSFC) (grant numbers 81720108031, 31721002, and 81872945), the Program for Introducing Talents of Discipline to the Universities of the Ministry of Education (grant number B08029), Key Program of Natural Science Foundation of Hubei Province (grant number 2019ACA128) and Wuhan (2019020701011481). P.C. were supported by the FUI of the French government (FUI, Cell2Lead project). J.G.M. was supported by the National Institutes of Health grants R01MH084894 and R01MH111940. Mouse picture in Figure 1 and Extended Data Fig. 3a was modified from Servier Medical Art (http://smart.servier.com/), licensed under a Creative

Common Attribution 3.0 Generic License (https://creativecommons.org/licenses/by/3.0/). Mouse brain in Extended Data Fig. 3a was from Figdraw (https://www.figdraw.com/). Pictures of the microplate in Figure 1 and Extended Data Fig. 3a were from Perkin Elmer Cisbio.

Author contributions

J.M. developed the FRET-based detectors and the FRET-based conformational change sensors, and performed the sensors experiments, IP_1 assays, co-immunoprecipitation and immunoblotting. C.X. proposed the idea and set up the protocol for the nanobody-based sensors for the detection of the expression and activation of mGlu2 in brain dissociated cells, and performed the DN1-DN10 sensor experiments in HEK-293 cells and brain dissociated cells and IP_1 assays. P.-A. performed the tissue immunofluorescence. S.R. designed and performed experiments with the FRET-based detectors and conformational change sensors. M.M. performed TR-FRET microscopy imaging, nanobody production, purification and labeling. R.Z. performed nanobody production, purification, labeling and co-immunoprecipitation. P.S. and E.B. developed the FRET-based conformational change biosensor for the mGlu2 homodimer in HEK-293 cells. J.A.J.B. and J.L.M. provided brain samples and trained J.M. for brain samples preparation. J.G.-M. prepared brain samples for the wild-type and mGlu2 KO mice. P.C. screened for the mGlu2 and mGlu4 nanobodies, and prepared the Fc versions. J.L., J.-P.P. and P.R. conceived experiments, supervised the work and wrote the manuscript.

Competing interests

P.R. and J.-P.P. are funded by Perkin Elmer CisBio through the collaborative laboratory Eidos. The remaining authors declare no competing interests.

Figure legends

Fig. 1 | Nanobody-based sensors to detect the expression and activation of endogenous membrane proteins. Schemes illustrating the design of two kinds of extracellular nanobody-based sensors either to detect membrane protein subunit assembly or their conformational change upon activation. These sensors are compatible with the detection of endogenous membrane proteins in dissociated cells from different mouse brain regions.

Fig. 2 | A nanobody-based biosensor to detect the expression and activation of the mGlu2 receptor in both transfected cells and dissociated brain tissues. (**a**) Schematic representation of the TR-FRET-based mGlu2 receptor conformational sensor in presence of the agonist or antagonist to stabilize the active and inactive states, respectively. This sensor was made of 7.5 nM donor nanobody DN1-Tb is in pink (Lumi4-Tb shown as a circled "D") and 15 nM acceptor nanobody DN10-d2 in purple (d2 shown as a circled "A"). (**b**) TR-FRET signal measured in mGlu2 transiently transfected HEK-293 cells or in mock cells in presence of the biosensor with agonist LY379268 (1 μM) or antagonist LY341495 (10 μM). Data are represented as mean ± SEM of triplicate measurements in three independent experiments. (**c**) Analysis of the relative expression of mGlu2 receptor in brain tissues in the presence of LY379268 (1 μM). TR-FRET signal indicated the slope values of the relative linear quantification experiments. Each dot represents a TR-FRET experiment performed on the indicated brain tissue of one mouse (n=5 for all samples of wild-type mice, n=2 for cerebellum of mGlu2 KO mice group and n=3 for cerebellum of mGlu4 KO mice group). Data are mean ± SEM and analyzed using one-way ANOVA followed by Dunnett's *post-hoc* test (compared with the cerebellum of mGlu2 KO group), with $****P < 0.0001$ for all, except for midbrain ($**P = 0.0044$). (**d and g-i**) Dose-dependent effects of the ligands on the TR-FRET signal of the biosensor measured in HEK-293 cells transiently co-transfected with mGlu2 and the high affinity glutamate transporter EAAC1 (*d*) or in dissociated cells from the cortex (*g*),

hippocampus (*h*), or cerebellum (*i*). (**e**) Dose-dependent effects of the indicated ligands on IP_1 accumulation measured on HEK-293 cells co-transfected with mGlu2, EAAC1, and the chimeric G protein Gqi9. In *d-e* and *g-i*, data are mean ± SEM of three independent experiments performed in triplicate and normalized to the response of LY379268. (**f**) Correlation between the potencies (pEC_{50}) determined with the indicated agonists on the conformational biosensor (*d*) and IP_1 assay (*e*). Data are mean ± SEM of three independent experiments.

Fig. 3 | Relative quantification of endogenous mGlu2 and mGlu4 homodimers by FRET. (**a and d**) Schematic representation of mGlu2 *(a)* and mGlu4 *(d)* homodimer that can be detected by FRET-based "detectors". mGlu2 homodimer "detector" *(a)* was made of donor and acceptor labeled nanobodies (DN1-Tb and DN1-d2 both at 25 nM). mGlu4 homodimer "detector" *(d)* was made of DN42-Tb and DN42-d2 (both at 1.6 nM). (**b and e**) TR-FRET signal measured in HEK-293 cells transfected with the mGlu2 *(b)* or mGlu4 receptors *(e)*, or in mock cells with the indicated "detectors" and the agonist LY379268 (1 µM) *(b)* or L-AP4 (100 µM) *(e)* and the antagonist LY341495 (10 µM). (**c and f**) TR-FRET signal measured in HEK-293 cells transfected with the indicated mGlu receptors or in mock cells with LY341495 (10 µM). In *b, e* and *c, f*, data are mean ± SEM of triplicate measurements from one representative experiment in three independent experiments. (**g and h**) Relative expression of the mGlu2 *(g)* and mGlu4 *(h)* homodimers in the indicated brain tissues by their respective "detectors". TR-FRET signal indicated the slope values of the relative linear quantification experiments. Each dot represents a TR-FRET measurement from one mouse (n=5 for all sample of wild-type mice, n=2 for cerebellum of mGlu2 KO mice group and n=3 for cerebellum of mGlu4 KO mice group). Data are mean ± SEM and analyzed using a one-way ANOVA followed by a Dunnett's *post-hoc* test (control group is the cerebellum of mGlu2 KO group (*g*), with $****P < 0.0001$ for all, except for striatum ($*P = 0.0164$) and midbrain (ns $P = 0.9996$) or mGlu4 KO group (*insert h*), with ns $P > 0.05$ for olfactory bulb (> 0.9999),

striatum (0.0896), hippocampus (0.8253) and midbrain (0.0615) and prefrontal cortex (**P = 0.0031), or a Welch's ANOVA test followed by a Dunnett's T3 *post-hoc* test (compared with the cerebellum of mGlu4 KO group) (*h*), with ns $P > 0.05$ for olfactory bulb (> 0.9999), striatum (0.2251), hippocampus (0.8436) and midbrain (0.1304) and *$P < 0.05$ for prefrontal cortex (0.0425) and the cerebellum of the wild-type group (0.0435).

Fig. 4 | Relative quantification of the mGlu2-4 heterodimer by FRET. (**a, b**) Schematic representation of the FRET-based "detector" for the mGlu2-4 heterodimer with mGlu2$_{C1}$ and mGlu4$_{C2}$ *(a)* or wild-type mGlu2 and mGlu4 are co-expressed *(b)*. This "detector" is made of DN42-Tb (1.6 nM) and DN1-d2 (25 nM). (**c, d**) TR-FRET signal measured in HEK-293 cells transiently transfected with mGlu2$_{C1}$ and mGlu4$_{C2}$ *(c)*, or co-transfected with both wild-type mGlu2 and mGlu4 *(d)* or on mock cells in presence of the "detector" with LY379268 (1 μM) or LY341495 (10 μM). Data are mean ± SEM of triplicate measurements from one representative experiment in three independent experiments. (**e–g**) Relative expression of the mGlu2-4 heterodimer in the indicated brain tissues by the "detector". TR-FRET signal indicated the slope values of the relative linear quantification experiments. Each dot represents a TR-FRET experiment performed on the indicated brain tissue of one mouse. For *e*, n=5 for all sample of wild-type mice except for the olfactory bulb (n=4), and cerebellum of mGlu4 KO mice group (n=3). For *f*, n=3 for the olfactory bulb of wild-type, mGlu2 KO and mGlu4 KO. For *g*, cerebellum of wild-type mice (n=8), mGlu2 KO (n=3) and mGlu4 KO mice (n=6). Data are mean ± SEM and analyzed using a one-way ANOVA followed by a Dunnett's *post-hoc* test, compared with the cerebellum of mGlu4 KO group (*e*), with ****$P < 0.0001$ for olfactory bulb and prefrontal cortex, **$P < 0.01$ for striatum (0.0054), hippocampus (0.0062), cerebellum (0.0045) and ns $P > 0.05$ for midbrain (0.1533); compared with the olfactory bulb of mGlu4 KO group (*f*), with ***$P < 0.001$ for wild-type group (0.0002) and ns $P > 0.05$ for

mGlu2 KO group (0.8100); or compared with the cerebellum of the wild-type group (*g*), with ns $P > 0.05$ for mGlu2 KO group (0.4120), ***$P < 0.001$ for mGlu4 KO group (0.0005).

Fig. 5 | A conformational biosensor detects the activation of the endogenous mGlu2-4 heterodimer. (**a and d**) Schematic representation of the conformational biosensor for the mGlu2-4 heterodimer when the $mGlu2_{C1}$ and $mGlu4_{C2}$ constructs are used to have only the heterodimer at the surface *(a)* or when wild-type mGlu2 and mGlu4 are co-expressed *(d)* in the presence of the indicated mGlu2 and mGlu4 agonists and antagonist. This biosensor is made of DN42-Tb (1.6 nM) and DN10-d2 (25 nM). (**b, e and h**) TR-FRET signal measured in HEK-293 cells co-transfected with $mGlu2_{C1}$ and $mGlu4_{C2}$ *(b)*, or with wild-type mGlu2 and mGlu4 *(e)* or the dissociated cells from the olfactory bulb *(h)* with the biosensor and the agonists LY379268 (1 µM) or L-AP4 (100 µM) and/or the antagonist LY341495 (10 µM). Data are analyzed using a One-way ANOVA followed by a Tukey's *post-hoc* test, with **** $P \leqslant 0.0001$ and ns $P > 0.05$. For *b* and *e*, data are mean ± SEM of four independent experiments performed in triplicate and normalized to the response of LY341495 (0%) and LY379268 (100%). For *h*, data are mean ± SEM of triplicate measurements from one representative experiment in three independent experiments. (**c, f and i**) Dose-dependent effects of the indicated ligands on the TR-FRET signal of the biosensor measured in HEK-293 cells co-transfected with $mGlu2_{C1}$ and $mGlu4_{C2}$ *(c)* or with both wild-type mGlu2 and mGlu4 *(f)*, or in the dissociated cells from the olfactory bulb *(i)*. Data are mean ± SEM of *n* independent experiments performed in duplicate (*c and f*, n=3) or in triplicate (*i*, n=5) and normalized to the response of LY379268. (**g**) TR-FRET signal of the biosensor where the ratio in the presence of LY379268 (1 µM) and LY341495 (10 µM) is measured. Each dot represents one measurement on the indicated brain tissue of WT or mGlu4 KO mouse (n=4, except the striatum group of mGlu4 KO (n=3)). Data are analyzed using two-tailed Student's t test, with ****$P \leqslant 0.0001$, **$P \leqslant 0.01$, *$P \leqslant 0.05$, and ns $P > 0.05$, and the exact P values have been indicated.

Fig. 6 | mGlu2-4 heterodimers are predominant over the mGlu4 homodimers outside the cerebellum. (a) Relative quantification of mGlu4-4 homodimers and mGlu2-4 heterodimers based on the TR-FRET signal between the two subunits in the dimer using either the SNAP- or CLIP-tag fluorescent substrates or the "detector" nanobodies. Data are mean ± SEM of triplicate measurements from one out of three experiments. **(b)** Relative amounts of the mGlu4 homodimer compared with the mGlu2-4 heterodimer, as indicated by the respective circle size, in the adult mouse brain according to the quantification with their respective "detectors". The relative amounts of the mGlu2 homodimer determined with its "detector" are indicated in a separate brain since the sensitivity of this detector is different.

References

1. Kniazeff, J., Prezeau, L., Rondard, P., Pin, J.P. & Goudet, C. Dimers and beyond: The functional puzzles of class C GPCRs. *Pharmacol Ther* **130**, 9-25 (2011).
2. Lemmon, M.A. & Schlessinger, J. Cell signaling by receptor tyrosine kinases. *Cell* **141**, 1117-1134 (2010).
3. Paoletti, P., Bellone, C. & Zhou, Q. NMDA receptor subunit diversity: impact on receptor properties, synaptic plasticity and disease. *Nat Rev Neurosci* **14**, 383-400 (2013).
4. Albizu, L. et al. Time-resolved FRET between GPCR ligands reveals oligomers in native tissues. *Nat Chem Biol* **6**, 587-594 (2010).
5. Rosenbaum, M.I., Clemmensen, L.S., Bredt, D.S., Bettler, B. & Stromgaard, K. Targeting receptor complexes: a new dimension in drug discovery. *Nat Rev Drug Discov* **19**, 884-901 (2020).
6. Schwenk, J. et al. Modular composition and dynamics of native GABAB receptors identified by high-resolution proteomics. *Nat Neurosci* **19**, 233-242 (2016).
7. Yu, J. et al. Hippocampal AMPA receptor assemblies and mechanism of allosteric inhibition. *Nature* **594**, 448-453 (2021).
8. Shi, Y. et al. A novel proximity assay for the detection of proteins and protein complexes: quantitation of HER1 and HER2 total protein expression and homodimerization in formalin-fixed, paraffin-embedded cell lines and breast cancer tissue. *Diagn Mol Pathol* **18**, 11-21 (2009).
9. Trifilieff, P. et al. Detection of antigen interactions ex vivo by proximity ligation assay: endogenous dopamine D2-adenosine A2A receptor complexes in the striatum. *Biotechniques* **51**, 111-118 (2011).
10. Sebastianutto, I. et al. D1-mGlu5 heteromers mediate noncanonical dopamine signaling in Parkinson's disease. *J Clin Invest* **130**, 1168-1184 (2020).
11. Gaborit, N. et al. Time-resolved fluorescence resonance energy transfer (TR-FRET) to analyze the disruption of EGFR/HER2 dimers: a new method to evaluate the efficiency of targeted therapy using monoclonal antibodies. *J Biol Chem* **286**, 11337-11345 (2011).
12. Zwier, J.M., Bazin, H., Lamarque, L. & Mathis, G. Luminescent lanthanide cryptates: from the bench to the bedside. *Inorg Chem* **53**, 1854-1866 (2014).
13. Nevoltris, D. et al. Conformational nanobodies reveal tethered epidermal growth factor receptor involved in EGFR/ErbB2 predimers. *ACS Nano* **9**, 1388-1399 (2015).
14. Mujic-Delic, A., de Wit, R.H., Verkaar, F. & Smit, M.J. GPCR-targeting nanobodies: attractive research tools, diagnostics, and therapeutics. *Trends Pharmacol Sci* **35**, 247-255 (2014).
15. Scholler, P. et al. Allosteric nanobodies uncover a role of hippocampal mGlu2 receptor homodimers in contextual fear consolidation. *Nat Commun* **8**, 1967 (2017).
16. Ma, Y. et al. Structure-guided discovery of a single-domain antibody agonist against human apelin receptor. *Sci Adv* **6**, eaax7379 (2020).
17. Haubrich, J. et al. A nanobody activating metabotropic glutamate receptor 4 discriminates between homo- and heterodimers. *Proc Natl Acad Sci U S A* **118** (2021).
18. Jahnichen, S. et al. CXCR4 nanobodies (VHH-based single variable domains) potently inhibit chemotaxis and HIV-1 replication and mobilize stem cells. *Proceedings of the National Academy of Sciences of the United States of America* **107**, 20565-20570 (2010).
19. McMahon, C. et al. Synthetic nanobodies as angiotensin receptor blockers. *Proc Natl Acad Sci U S A* **117**, 20284-20291 (2020).

20. Niswender, C.M. & Conn, P.J. Metabotropic glutamate receptors: physiology, pharmacology, and disease. *Annu Rev Pharmacol Toxicol* **50**, 295-322 (2010).
21. El Moustaine, D. et al. Distinct roles of metabotropic glutamate receptor dimerization in agonist activation and G-protein coupling. *Proc Natl Acad Sci U S A* **109**, 16342-16347 (2012).
22. Koehl, A. et al. Structural insights into the activation of metabotropic glutamate receptors. *Nature* **566**, 79-84 (2019).
23. Levitz, J. et al. Mechanism of Assembly and Cooperativity of Homomeric and Heteromeric Metabotropic Glutamate Receptors. *Neuron* **92**, 143-159 (2016).
24. Lin, S. et al. Structures of Gi-bound metabotropic glutamate receptors mGlu2 and mGlu4. *Nature* **594**, 583-588 (2021).
25. Seven, A.B. et al. G-protein activation by a metabotropic glutamate receptor. *Nature* **595**, 450-454 (2021).
26. Doumazane, E. et al. A new approach to analyze cell surface protein complexes reveals specific heterodimeric metabotropic glutamate receptors. *FASEB J* **25**, 66-77 (2011).
27. Moreno Delgado, D. et al. Pharmacological evidence for a metabotropic glutamate receptor heterodimer in neuronal cells. *Elife* **6** (2017).
28. Xiang, Z. et al. Input-specific regulation of glutamatergic synaptic transmission in the medial prefrontal cortex by mGlu2/mGlu4 receptor heterodimers. *Sci Signal* **14** (2021).
29. Yin, S. et al. Selective actions of novel allosteric modulators reveal functional heteromers of metabotropic glutamate receptors in the CNS. *J Neurosci* **34**, 79-94 (2014).
30. Lee, J. et al. Defining the Homo- and Heterodimerization Propensities of Metabotropic Glutamate Receptors. *Cell Rep* **31**, 107891 (2020).
31. Ferraguti, F. & Shigemoto, R. Metabotropic glutamate receptors. *Cell Tissue Res* **326**, 483-504 (2006).
32. Wright, R.A. et al. CNS distribution of metabotropic glutamate 2 and 3 receptors: transgenic mice and [(3)H]LY459477 autoradiography. *Neuropharmacology* **66**, 89-98 (2013).
33. Doumazane, E. et al. Illuminating the activation mechanisms and allosteric properties of metabotropic glutamate receptors. *Proc Natl Acad Sci U S A* **110**, E1416-1425 (2013).
34. Scholler, P. et al. HTS-compatible FRET-based conformational sensors clarify membrane receptor activation. *Nat Chem Biol* **13**, 372-380 (2017).
35. Cao, A.M. et al. Allosteric modulators enhance agonist efficacy by increasing the residence time of a GPCR in the active state. *Nat Commun* **12**, 5426 (2021).
36. Liu, J. et al. Allosteric control of an asymmetric transduction in a G protein-coupled receptor heterodimer. *Elife* **6** (2017).
37. Asher, W.B. et al. Single-molecule FRET imaging of GPCR dimers in living cells. *Nat Methods* **18**, 397-405 (2021).
38. Moller, T.C. et al. Oligomerization of a G protein-coupled receptor in neurons controlled by its structural dynamics. *Sci Rep* **8**, 10414 (2018).
39. Kinoshita, A. et al. Presynaptic localization of a metabotropic glutamate receptor, mGluR4a, in the cerebellar cortex: a light and electron microscope study in the rat. *Neurosci Lett* **207**, 199-202 (1996).
40. Neki, A. et al. Metabotropic glutamate receptors mGluR2 and mGluR5 are expressed in two non-overlapping populations of Golgi cells in the rat cerebellum. *Neuroscience* **75**, 815-826. (1996).
41. Chorev, D.S. & Robinson, C.V. The importance of the membrane for biophysical measurements. *Nat Chem Biol* **16**, 1285-1292 (2020).

42. Oliveira, S., Heukers, R., Sornkom, J., Kok, R.J. & van Bergen En Henegouwen, P.M. Targeting tumors with nanobodies for cancer imaging and therapy. *J Control Release* **172**, 607-617 (2013).
43. Faklaris, O. et al. Multicolor time-resolved Forster resonance energy transfer microscopy reveals the impact of GPCR oligomerization on internalization processes. *FASEB J* **29**, 2235-2246 (2015).
44. Werthmann, R.C. et al. Symmetric signal transduction and negative allosteric modulation of heterodimeric mGlu1/5 receptors. *Neuropharmacology* **190**, 108426 (2021).
45. Prezeau, L. et al. Functional crosstalk between GPCRs: with or without oligomerization. *Curr Opin Pharmacol* **10**, 6-13 (2010).
46. Grushevskyi, E.O. et al. Stepwise activation of a class C GPCR begins with millisecond dimer rearrangement. *Proc Natl Acad Sci U S A* **116**, 10150-10155 (2019).
47. Marek, G.J. Metabotropic glutamate2/3 (mGlu2/3) receptors, schizophrenia and cognition. *Eur J Pharmacol* **639**, 81-90 (2010).
48. Marino, M.J. et al. Allosteric modulation of group III metabotropic glutamate receptor 4: a potential approach to Parkinson's disease treatment. *Proc Natl Acad Sci U S A* **100**, 13668-13673 (2003).
49. Rosemond, E. et al. Molecular basis for the differential agonist affinities of group III metabotropic glutamate receptors. *Mol Pharmacol* **66**, 834-842 (2004).
50. Niswender, C.M. et al. Context-dependent pharmacology exhibited by negative allosteric modulators of metabotropic glutamate receptor 7. *Mol Pharmacol* **77**, 459-468 (2010).

Materials and Methods

Animal ethics

This project followed the Animal Welfare Body guidelines and was approved by the internal Ethics Committee of the Institut de Génomique Fonctionnelle (Montpellier, France). Wild-type mice were purchased from Janvier Labs (Le Genest-Saint-Isle, France), knock-out mGlu2 mice[51] were kindly provided by Dr. Gonzalez Maeso (Virginia Commonwealth University School of Medicine, Richmond, VA, USA), while knock-out mGlu4 mice[52] were available at the Institut de Génomique Fonctionnelle (Montpellier, France). Animals were housed under a 12 h light/dark cycle at 23 ± 2°C with a relative humidity of 53 ± 10%. Mice had access to water and food *ad libitum*.

Reagents, cell lines, and plasmids

DCG-IV, LY341495, LY379268, and LY354740 were purchased from Tocris Bioscience (Bristol, UK). Glutamate was purchased from Sigma-Aldrich (Saint Louis, MO, USA). LSP4-2022 was provided by Dr. F. Acher (Paris, France). Anti-c-Myc-d2, anti-6His-d2, SNAP-Lumi4-Tb, Lumi4-Tb-NHS, d2-NHS, and Tag-lite® buffer were kindly supplied by Perkin Elmer Cisbio (Codolet, France).

HEK-293 cells (ATCC, CRL-1573, lot: 3449904) were cultured in DMEM (Thermo Fischer Scientific, Courtaboeuf, France) supplemented with 10% (v/v) fetal bovine serum (FBS, Sigma-Aldrich) at 37°C and 5% CO_2. HEK-293F cells were cultured in suspension in SMM 293-TI animal-free and serum-free at 37°C and 5% CO_2 with shaking at 200 rpm to produce nanobodies Fc-DN42 or Fc-GFP. The absence of mycoplasma was routinely checked using the MycoAlert Mycoplasma Detection Kit (Lonza, Amboise, France), in accordance with the manufacturer's protocol.

The pRK5 plasmids encoding wild-type rat mGlu1-8, with the HA- and SNAP-tags next to the human mGlu5 signal peptide, have been described previously [26]. For the quality control system, we used the mGlu2/4 C1 or C2 plasmids tagged with HA or Flag, with or without SNAP tags [36]. The sequence coding for C1 and C2 contains the coiled-coil region of the C terminus of $GABA_{B1a}$ or $GABA_{B2}$, and the endoplasmic reticulum retention signal KKTN, which allows to control the trafficking of the constructs to the cell surface. The other plasmids, namely the glutamate transporter EAAC1 and the chimeric G protein $G\alpha_{qi9}$, were previously described [26].

To construct the cDNA of the Fc-DN42 and Fc-GFP nanobodies [53], the monomeric DN42 and anti-GFP sequences were subcloned into pcDNA3.1 (+). The secreted signal peptide of human interleukin (IL-2) was introduced before the N-terminal of the nanobody, allowing the secretion of the protein into the culture medium. The C-terminus of the nanobody was fused with the sequence encoding the Fc region of human immunoglobulin IgG_1. The 6xHis tagged sequence

was fused at the C-terminus for the purification and separation of nanobodies by affinity chromatography with metal chelation.

Library construction and DN42 selection

DN42 targeting the mGlu4 subunit was selected from the V_HH library after all the procedures including the llama immunization, library construction, and selection of nanobodies targeting mGlu4 were performed as described previously [17].

Bacteria were then infected with the KM13 helper phage, and phage-containing pellets were purified by two selection rounds on rat mGlu4 receptor transfected into 2×10^7 HEK-293T cells. Each round was preceded by a depletion step on cells that were not transfected, and positive selection was performed in the presence of an excess of anti-HEK-293 cells. *E. coli* TG1 bacteria were infected with eluted phages and used for the sequencing and production of the nanobody.

Production and purification of nanobodies

For the nanobodies DN1 and DN10, production and purification were performed as previously described [15]. Briefly, a *E. coli* BL21DE3 colony transformed with the pHEN phagemid carrying cDNA of the nanobody of interest was grown in LB medium. The bacteria were cultured in large scale at 37°C and the expression of the nanobody was induced by 1 mM IPTG at 28°C. Bacteria were then collected after centrifugation and treated with different buffers to extract the periplasmic proteins. Nanobody in the periplasmic space was collected from the supernatant after a centrifugation at 4°C.

For large-scale production of the Fc-DN42 and Fc-GFP nanobodies, HEK-293F cells were cultured at a density of 0.6×10^6 mL^{-1} with 180 mL fresh medium in a 2 L culture bottle at 37°C and 5% CO_2, shaken at 200 rpm. Of the cells, $1–1.5 \times 10^6$ mL^{-1} were transfected with a mixture of Fc-DN42 or Fc-GFP plasmids (225 µg in 12 mL OMEM) and PEI (675 µg in 12

mL OMEM). Cells were cultured for 4–7 days at 37°C and 5% CO_2 with 200 rpm shaking. The supernatant was collected after a 10-min centrifugation at 2,000 × g and 4°C.

The His-tagged nanobodies from both bacteria and HEK-293F cells were then purified from the supernatant using Ni-NTA purification (Qiagen, Hilden, Germany) in accordance with the manufacturer's instructions. Finally, the nanobodies were purified by size-exclusion chromatography on a Superdex 200 10/300 column for Fc-DN42 and Fc-GFP, and Superdex 75 10/300 column for DN1 and DN10 (GE Healthcare, UK) in phosphate buffer saline (PBS, pH = 7.4).

Nanobody labeling

Nanobodies were dialyzed overnight at 4°C and incubated (250 µg of nanobodies per 2 mg mL^{-1}) at 20°C with d2-NHS (Perkin Elmer Cisbio) in 0.1 M carbonate buffer (pH = 9) and Lumi4-Tb-NHS in 50 mM phosphate buffer (pH = 8) at a molar ratio of 6 or 12 for 45 or 30 min, respectively. The nanobodies were then purified using a gel filtration column (NAP-5, GE Healthcare) in 100 mM phosphate buffer (pH = 7). The final molar ratio, namely the number of fluorophores per nanobodies, was calculated as the fluorophore concentration/conjugated nanobody concentration, and the conditions were set up for a ratio between 2 and 3 (for DN1 and DN10), 2 and 4 (for Fc-DN42 labeled with d2), or 5 and 8 (for Fc-DN42 labeled with Lumi4-Tb). The concentration of fluorophores in the labeled fraction was calculated as the OD/ε for each fluorophore (OD at 340 nm and ε = 26,000 M^{-1} cm^{-1} for Lumi4-Tb, and OD at 650 nm and ε = 225,000 M^{-1} cm^{-1} for d2), while that of nanobodies was determined by the OD at 280 nm (OD_{280}). The conjugated concentration was calculated as $OD_{280}-(OD_{fluo}/Rz_{max})/\varepsilon$ nanobody, with $Rz_{max} = OD_{fluo}/OD_{280}$. After purification, labeled nanobodies were supplemented with 0.1% bovine serum albumin (BSA) and stored at −20°C.

TR-FRET binding measurements

757 The FRET signal was determined by measuring the sensitized d2 acceptor emission (Em 665
758 nm) and Lumi4-Tb donor emission (Em 620 nm) using a 50 µs delay and 450 µs integration
759 upon excitation at 337 nm. All data were obtained using PHERAstar FS (BMG LabTech,
760 Ortenberg, Germany). The TR-FRET ratio was calculated as Em 665 nm/ Em 620 nm × 10^4 as
761 previously described [15].

762 HEK-293 cells were co-transfected with rat SNAP-tagged mGlu and EAAC1 (unless otherwise
763 indicated) using Lipofectamine in a 100 mm cell culture dish in accordance with the
764 manufacturer's instructions. Twenty-four hours after transfection, cells were plated in
765 polyornithine-coated, white 96-well plates (Greiner Bio-One) at 10^5 cells/well and cultured
766 overnight at 37°C and 5% CO_2 for adherent cell experiments. Cells were labeled with 100 nM
767 SNAP-Lumi4-Tb in DMEM-GlutaMAX (Thermo Fischer Scientific) for 2 h at 37°C, and then
768 washed three times with Krebs buffer (10 mM HEPES pH 7.4, 146 mM NaCl, 4.2 mM KCl, 1
769 mM $CaCl_2$, 0.5 mM $MgCl_2$, 5.6 mM glucose, and 0.1% BSA). For suspension experiments,
770 cells were frozen at −80°C with 10% DMSO and FBS, and then washed three times with Krebs
771 buffer before use. Five microliters of cells were plated in a white, small volume 384-well plate
772 (Greiner Bio-One) at 2 × 10^4 cells/well.

773 To determine the selectivity of Fc-DN42 for the mGlu1–8 receptors, 100 nM of nanobody and
774 200 nM of anti-His antibody labeled with d2, and the agonists (1 µM quisqualic acid for mGlu1;
775 5 or 100 µM L-AP4 for mGlu4, 6, 7, and 8; 100 nM LY379268 for mGlu2 and 3), or the
776 antagonist (10 µM LY341495) were applied to labeled cells in adherent cell experiments, with
777 a total volume of 60 µL per well. After an overnight incubation at 25°C, the TR-FRET signal
778 between Lumi4-Tb and d2 was determined.

779 To determine the affinity of the c-Myc-tagged nanobodies (DN1 and DN10) and His-tagged
780 nanobody Fc-DN42, 200 nM of anti-c-Myc and 100 nM of anti-His antibodies, both labeled

781 with d2, were used. The different reagents were applied to labeled cells in adherent or
782 suspension experiments, with a total volume of 20 µL per well incubated overnight at 25°C.
783 The TR-FRET signal between Lumi4-Tb and d2 was determined.

784 **SNAP subunit quantification**

785 Transfected HEK-293 cells were plated in polyornithine-coated, white 96-well plates (Greiner
786 Bio-One) at 10^5 cells/well and cultured overnight at 37°C and 5% CO_2; the cells were then
787 labeled with 100 nM SNAP-Lumi4-Tb in DMEM-GlutaMAX for 2 h at 37 °C, followed by
788 three washes with Krebs buffer. The signal was determined by measuring the emission intensity
789 of Lumi4-Tb at 620 nm with a 50 µs delay and 450 µs integration upon excitation at 337 nm.
790 All data were obtained using a PHERAstar FS (BMG LabTech, Ortenberg, Germany).

791 **Tissue cell sample preparation**

792 To obtain dissociated cells from brain tissue, 6–8 weeks-old C57BL/6 mice (including wild-
793 type or *Grm4*$^{-/-}$ male and female) were euthanized; the whole brain was dissected in cold PBS
794 (pH = 7.4) to obtain the regions of interest, according to the Allen Mouse Brain Atlas
795 (https://mouse.brain-map.org/) [54]. Tissues were quickly cut into small pieces using a scalpel,
796 collected into a 1.5 mL cryogenic tube (Thermo Fisher Scientific Nalgene system 100TM,
797 Boston, MA, USA) in 1 mL of cold cryopreservation medium (DMEM GlutaMAX
798 supplemented with 10% FBS and 10% DMSO), frozen at −80°C in a freezing box, and stored
799 at −80°C if not used immediately. When tissues were needed, the samples were rapidly thawed
800 in a water bath at 37°C. The cryopreservation medium was replaced with a precooled medium
801 (DMEM-GlutaMAX supplemented with 10% FBS), and the tissues were washed with cold
802 PBS. Frozen tissues or fresh tissues were digested with 400 µL of Versene solution (Thermo
803 Fisher) for 10 min at 20°C, and the cells were dissociated by pipetting. Then, 200 µL of DMEM
804 supplemented with 10% FBS was added. After 5–8 min of incubation, the supernatant was

transferred into a new 2 mL tube. The remaining precipitate was resuspended in 300 µL DMEM GlutaMAX supplemented with 10% FBS. After 3 min of incubation, the supernatants were transferred and combined with the supernatant. This step was repeated two more times to obtain the largest number of dissociated cells. Finally, the total dissociated cells were centrifuged at 3,000 x g for 5 min, and the cell pellet was resuspended in 400 µL of cold PBS.

TR-FRET measurement with the nanobody-based sensors

For TR-FRET measurements in attached cells, transfected HEK-293 cells were plated in polyornithine-coated, white 96-well plates (Greiner Bio-One) at 10^5 cells/well and cultured overnight at 37°C and 5% CO_2. Cells were starved in DMEM-GlutaMAX for 2 h at 37°C, and then washed once with Krebs buffer to reduce ambient glutamate. Donor and acceptor nanobodies and ligands were prepared in Krebs buffer and added to the plate to reach a total volume of 60 µL per well. For TR-FRET measurements in cell suspensions, 5 µL of HEK-293 cells alone or transfected with mGlu receptor encoding plasmids were added to a low-volume 384-well microplate (Greiner Bio-One) at 2×10^4 cells/well. All reagents were added to reach a total volume of 20 µL per well. For TR-FRET measurements in dissociated brain cells, 10 µL of cells in PBS, corresponding to different amounts of total proteins, were added to a half-area 96-well microplate (Greiner Bio-One); all reagents were added to reach a total volume of 40 µL. In all cell preparations, the plates were incubated at 25°C for 4 h or overnight, then the TR-FRET signal was measured as previously described [15].

BCA assay for protein quantification

The dissociated cells (30 µL) in PBS were diluted twice with PBS containing 2% Triton X-100 and incubated at 20°C for 1 h. The total protein quantity was measured in triplicate using a bicinchoninic acid kit (BCA1, Sigma-Aldrich) in accordance with the manufacturer's instructions using Infinite F500® microplate reader (Tecan, Crailsheim, Germany).

Relative quantification of mGlu4-4 homodimer and mGlu2-4 heterodimer by TR-FRET

Twenty-four hours after transfection, cells (100,000 cells/well in a 96-well microplate) were labeled in Tris-Krebs buffer for 1 h at 37℃ and 5% CO_2 with the "detector" nanobodies (1.6 nM Fc-DN42-Tb and 1.6 nM Fc-DN42-d2 for the SNAP-tagged mGlu4 homodimer; 1.6 nM Fc-DN42-Tb and 25 nM DN1-d2 for the co-expressed wild-type CLIP-tagged mGlu2 and SNAP-tagged mGlu4 to obtain the mGlu2-4 heterodimer) or the SNAP/CLIP substrates (100 nM SNAP-Lumi4-Tb and 100 nM SNAP-d2 for the SNAP-tagged mGlu4 homodimer; 100 nM CLIP-Lumi4-Tb and 100 nM SNAP-d2 for the co-expressed wild-type CLIP-tagged mGlu2 and SNAP-tagged mGlu4). After labeling, the cells were washed thrice with Tris-Krebs buffer, and the signal was recorded with 100 µL of Tris-Krebs buffer per well. The TR-FRET signal was measured using a PHERAstar FS, by the emission of d2 at 665 nm with a 50 µs delay and a 450 µs integration time after excitation at 337 nm.

Measurements of inositol phosphate

HEK-293 cells were transiently co-transfected with the mGlu receptors, EAAC1, and the chimeric G_{qi9} protein using Lipofectamine 2000. Sixteen hours after transfection, the cells were incubated with the indicated ligands and 10 mM LiCl for 30 min. The accumulated inositol-phosphate-1 (IP_1) was quantified using a PHERAstar FS and the IP One HTRF assay kit (Perkin Elmer Cisbio, Codolet, France) in accordance with the manufacturer's instructions.

Neuronal culture and TR-FRET microscopy imaging

The primary hippocampal neurons were cultured following the procedures described previously[27], and after 17 days of culture, neurons were imaged. Neurons were labeled with 120 nM DN1-d2 and 80 nM DN10-Tb in the presence or absence of ligands (150 nM LY379268 or 1 µM LY341495) for 2 h at 37°C. After labeling by nanobodies, the neurons

were washed four times before imaging to remove the unbound nanobodies. Labeling and washing were performed in imaging buffer (127 mM NaCl, 2.8 mM KCl, 1.1 mM $MgCl_2$, 1.15 mM $CaCl_2$, 10 mM D-glucose, 10 mM HEPES, pH 7.3), supplemented with 1% BSA. Images were acquired with a homebuilt TR-FRET microscope[43], following a previously described protocol [27].

Brain collection and fixation

Mice were euthanized with 140 mg/kg sodium pentobarbital (Euthasol Vet®, Dômes Pharma Vétérinaire TVM, Lempdes, France) followed by cardiac perfusion with PBS. Brains were extracted and incubated overnight at 4°C in a 4% paraformaldehyde solution (Euromedex, Souffelweyersheim, France), cryoprotected for 4 days at 4°C with a 30% sucrose solution, included in an optimal cutting temperature compound (Tissue-Tek® O.C.T., Sakura Finetek, Villeneuve d'Ascq, France), and quickly frozen in ethanol cooled on dry ice. Brains were stored at −80°C until use. Frozen brains were mounted on a cryostat (Leica Biosystems, Nanterre, France) and 16 µm sagittal sections were obtained. Sections were mounted on Superfrost Plus glass slides (Microm France, Francheville, France) and kept at −20°C until use.

Tissue immunofluorescence

Fifteen to twenty sections per mouse (n = 2–3 per genotype) were used. Sections were rinsed in PBS and incubated for 1 h at 20°C with a blocking solution (3% BSA and 0.1% Triton X-100 in PBS). Sections were then incubated with the appropriate nanobody: 200 nM of DN1-d2 (overnight at 4 °C) or 300 nM of Fc-DN42-d2 (1.5 h at 20°C). Sections were first washed in PBS, then in distilled water, and mounted in Fluoroshield® mounting medium with DAPI (Sigma-Aldrich, Saint-Quentin-Fallavier, France). All images were taken with a slide scanner Axio scan Z1 microscope (Carl Zeiss Microscopy, Jena, Germany) by performing full-section mosaics at 20× magnification.

Co-immunoprecipitation and immunoblotting

The mice were decapitated, brains were rapidly removed, and the OB was separated. Samples from 4–5 mice were combined and homogenized in a tissue grinder with 10 μL lysis buffer (25 mM HEPES, 150 mM NaCl, 1.0% LMNG, protease inhibitor cocktail, pH 8.0) per mg of tissue and incubated for 1 h at 4 °C. The lysate was then centrifuged at 12,000 × g for 45 min at 4 °C, and the supernatant was collected. The lysate was precleared with protein A beads (Millipore 16-125, Sigma-Aldrich (Shanghai, China) for 2 h at 4°C. Fc-DN42 or Fc-GFP nanobodies were bound to protein A beads by rotating at 4°C for 3 h. The precleared lysate was then added to the antibody-bound protein A beads and incubated overnight at 4°C. The beads were washed four times with wash buffer (25 mM HEPES, 150 mM NaCl, 0.01% LMNG, protease inhibitor cocktail, pH 8.0), and proteins were eluted with unheated SDS sample buffer. Samples were subjected to SDS–PAGE using 10% polyacrylamide gels and then transferred to nitrocellulose membranes (GE Healthcare). After the transfer, membranes were blocked in TBST (25 mM Tris, 150 mM NaCl, and 0.1% Tween 20) containing 5% BSA at 20°C for 1 h. mGluR2 (Abcam, ab15672, Shanghai, China) and mGluR4 antibodies (Abcam, ab184302, Shanghai, China) were diluted 1:1,500 in blocking buffer and incubated with the membranes at 4°C overnight. Membranes were washed four times with TBST and then incubated in HRP-conjugated goat anti-mouse IgG secondary antibody (Cell Signaling Technology (CST),7076S, Massachusetts, USA) or incubated in HRP-conjugated goat anti-rabbit IgG secondary antibody (CST, 7074S) diluted 1:10,000 in TBST containing 5% nonfat milk for 1 h at 20°C. Membranes were then washed four times with TBST, and an enhanced chemiluminescent assay (Thermo Scientific) was performed to detect immunoreactive proteins. The membrane was scanned using an imager.

Statistical analysis

All data are presented as mean ± SEM and were initially analyzed using GraphPad Prism (version 9.1.2 for Windows, GraphPad software, San Diego, California, USA) using Shapiro-Wilk's normality test. Normally distributed data sets ($P > 0.05$) were analyzed using parametric tests, a two-tailed Student's t test or a one-way analysis of variance (ANOVA) followed by a Dunnett's or Tukey's *post-hoc* analysis, or a two-way ANOVA followed by a Tukey's *post-hoc* test, depending on the experiments analyzed. For data analyzed with the one-way ANOVA and having a significant Brown-Forsythe test ($P < 0.05$, meaning there is unequal variance between the different groups), data sets were analyzed using Welch's ANOVA test followed by Dunnett's T3 *post-hoc* test (recommended for n < 50 /group). For all statistical analyses, a probability of 0.05 has been defined as a significant difference. The exact P values were indicated in figures or in figure legends.

Data availability

All raw data of the main and extended Figures and Supplementary information are all included in the Data Source files. Materials and protocols are available on request.

References

51. Yokoi, M. et al. Impairment of hippocampal mossy fiber LTD in mice lacking mGluR2. *Science* **273**, 645-647 (1996).
52. Pekhletski, R. et al. Impaired cerebellar synaptic plasticity and motor performance in mice lacking the mGluR4 subtype of metabotropic glutamate receptor. *J Neurosci* **16**, 6364-6373 (1996).
53. Kubala, M.H., Kovtun, O., Alexandrov, K. & Collins, B.M. Structural and thermodynamic analysis of the GFP:GFP-nanobody complex. *Protein Sci* **19**, 2389-2401 (2010).
54. Lein, E.S. et al. Genome-wide atlas of gene expression in the adult mouse brain. *Nature* **445**, 168-176 (2007).

Graphical Abstract

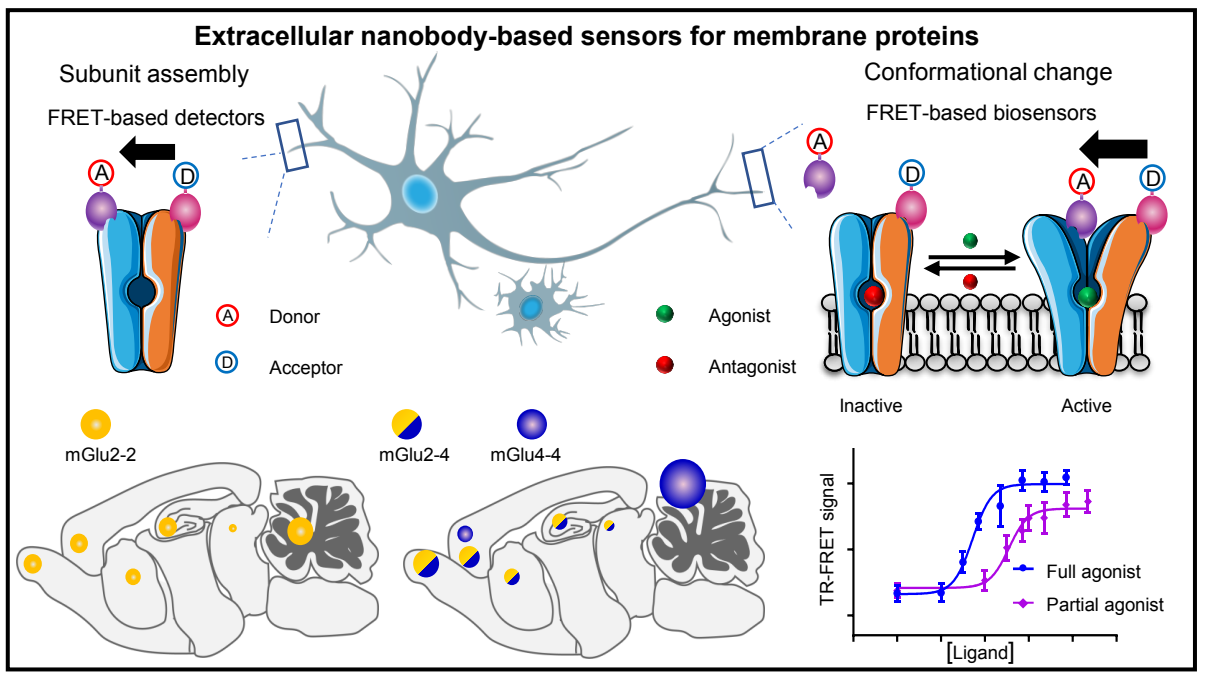

Main figures

Optical biosensors of native membrane protein complexes reveal high proportion of mGlu heterodimers in the brain

Jiyong Meng[a,b,c,*], Chanjuan Xu[a,c*], Pierre-André Lafon[a], Salomé Roux[b], Michaël Mathieu[b], Rui Zhou[a], Pauline Scholler[b], Emilie Blanc[b], Jérôme A. J. Becker[d], Julie Le Merrer[d], Javier González-Maeso[f], Patrick Chames[g], Jianfeng Liu[a,c,1] Jean-Philippe Pin[b,1] and Philippe Rondard[b,1]

[a] Cellular Signaling Laboratory, International Research Center for Sensory Biology and Technology of MOST, Key Laboratory of Molecular Biophysics of MOE, and College of Life Science and Technology, Huazhong University of Science and Technology, 430074 Wuhan, China.

[b] Institut de Génomique Fonctionnelle, Université de Montpellier, CNRS, INSERM, 34094 Montpellier Cedex 5, France.

[c] Guangzhou Regenerative Medicine and Health Guangdong Laboratory, 510005 Guangzhou, China.

[d] Physiologie de la Reproduction et des Comportements, INRAE UMR0085, CNRS UMR7247, IFCE, Université de Tours, INSERM, 37380 Nouzilly, France.

[e] UMR1253, iBrain, Université de Tours, INSERM, CNRS, 37200 Tours, France.

[e] Department of Physiology and Biophysics, Virginia Commonwealth University School of Medicine, Richmond, VA 23298, USA

[f] Institut Paoli-Calmettes, Aix Marseille University, CNRS, INSERM, CRCM, 13009 Marseille, France;

* Co-first authors.

[1] To whom correspondence may be addressed. Email: philippe.rondard@igf.cnrs.fr, jean-philippe.pin@igf.cnrs.fr or jfliu@mail.hust.edu.cn.

Figure 1.

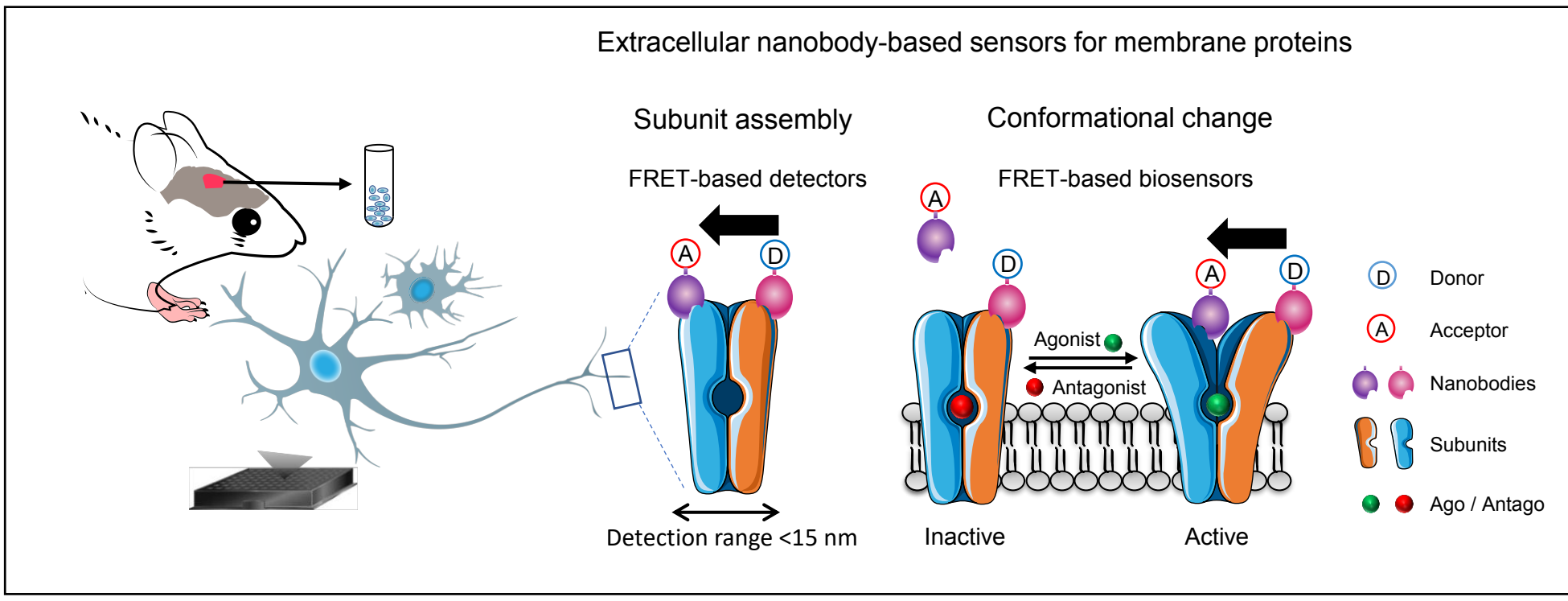
Extracellular nanobody-based sensors for membrane proteins
Subunit assembly
FRET-based detectors
A
D
Detection range <15 nm
Conformational change
FRET-based biosensors
A
D
Agonist
Antagonist
Inactive
Active
D Donor
A Acceptor
Nanobodies
Subunits
Ago / Antago

Figure 2. A nanobody-based biosensor to detect the expression and activation of the mGlu2 receptor both on transfected cells and cell dissociated brain tissues.

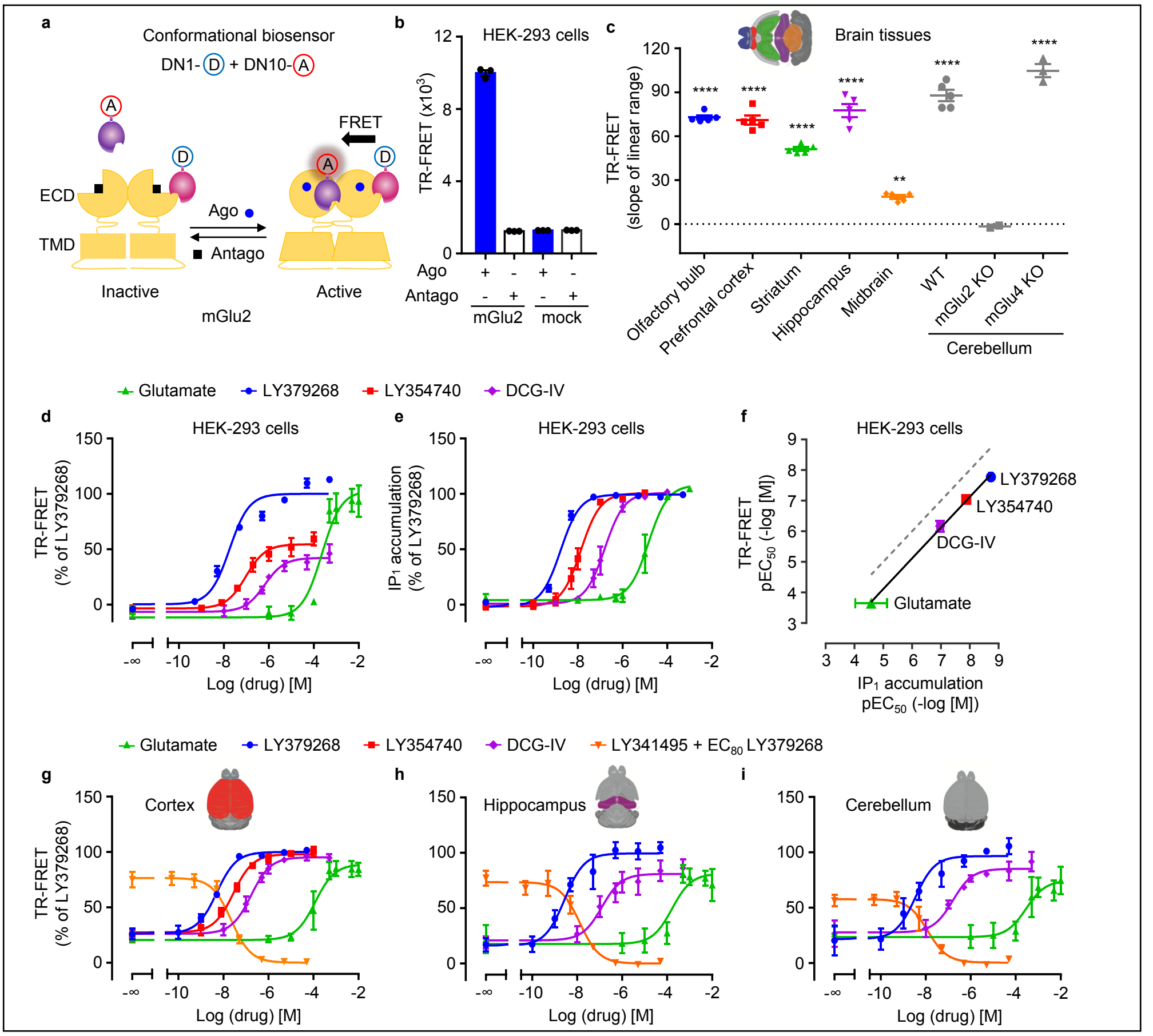

Figure 3. Relative quantification of endogenous mGlu2 and mGlu4 homodimers by FRET.

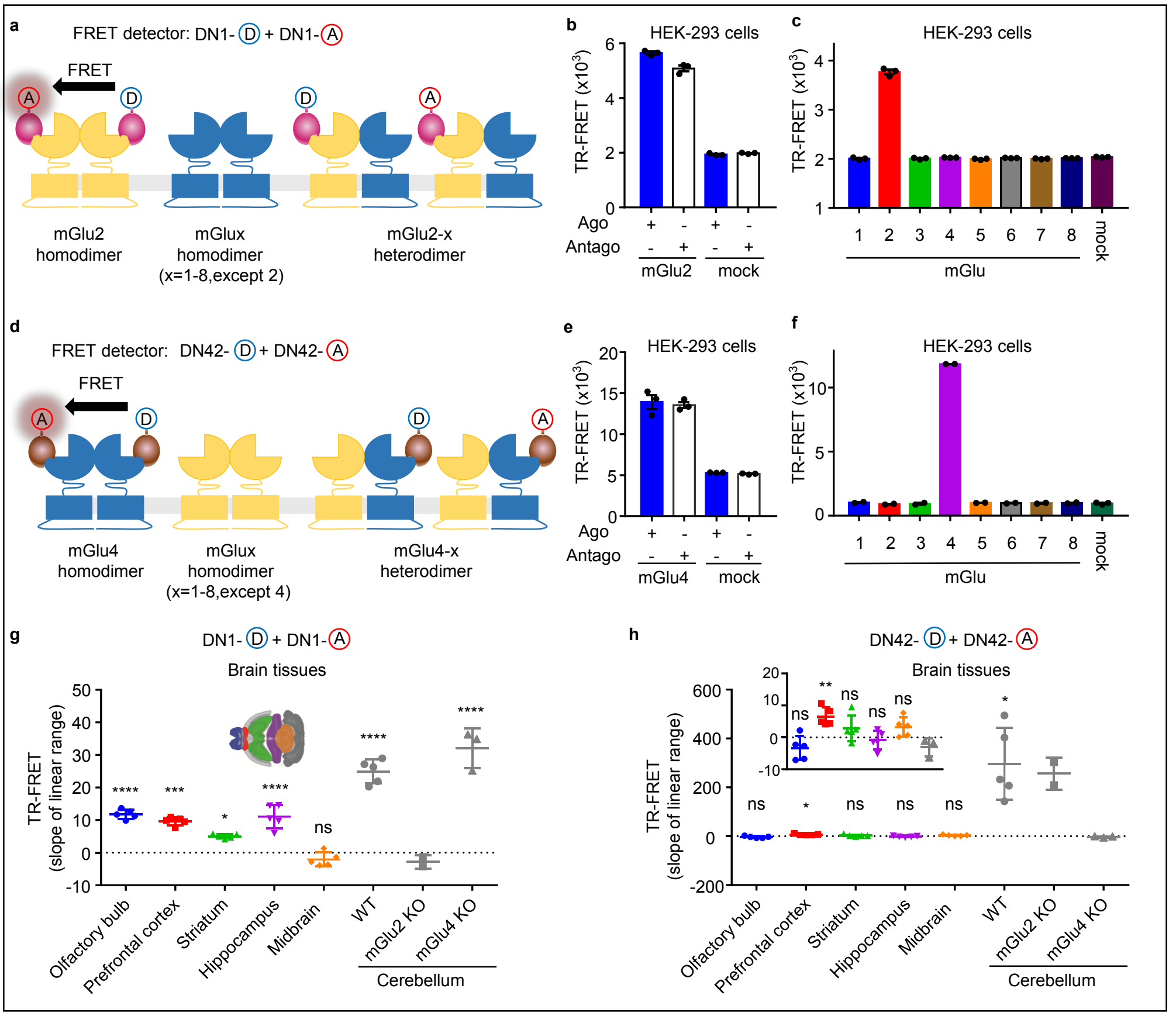

Figure 4. Relative quantification of the mGlu2-4 heterodimer by FRET.

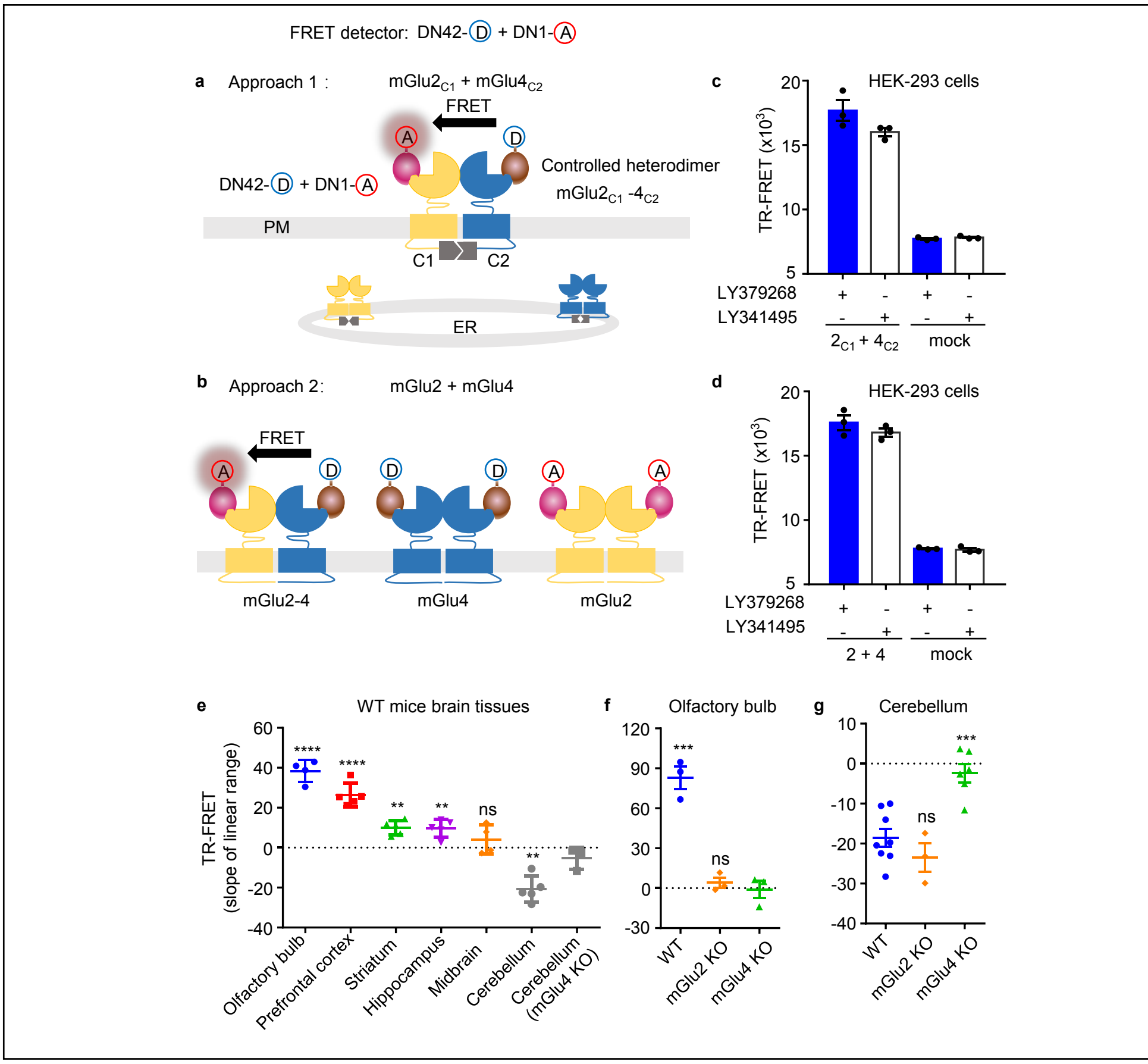

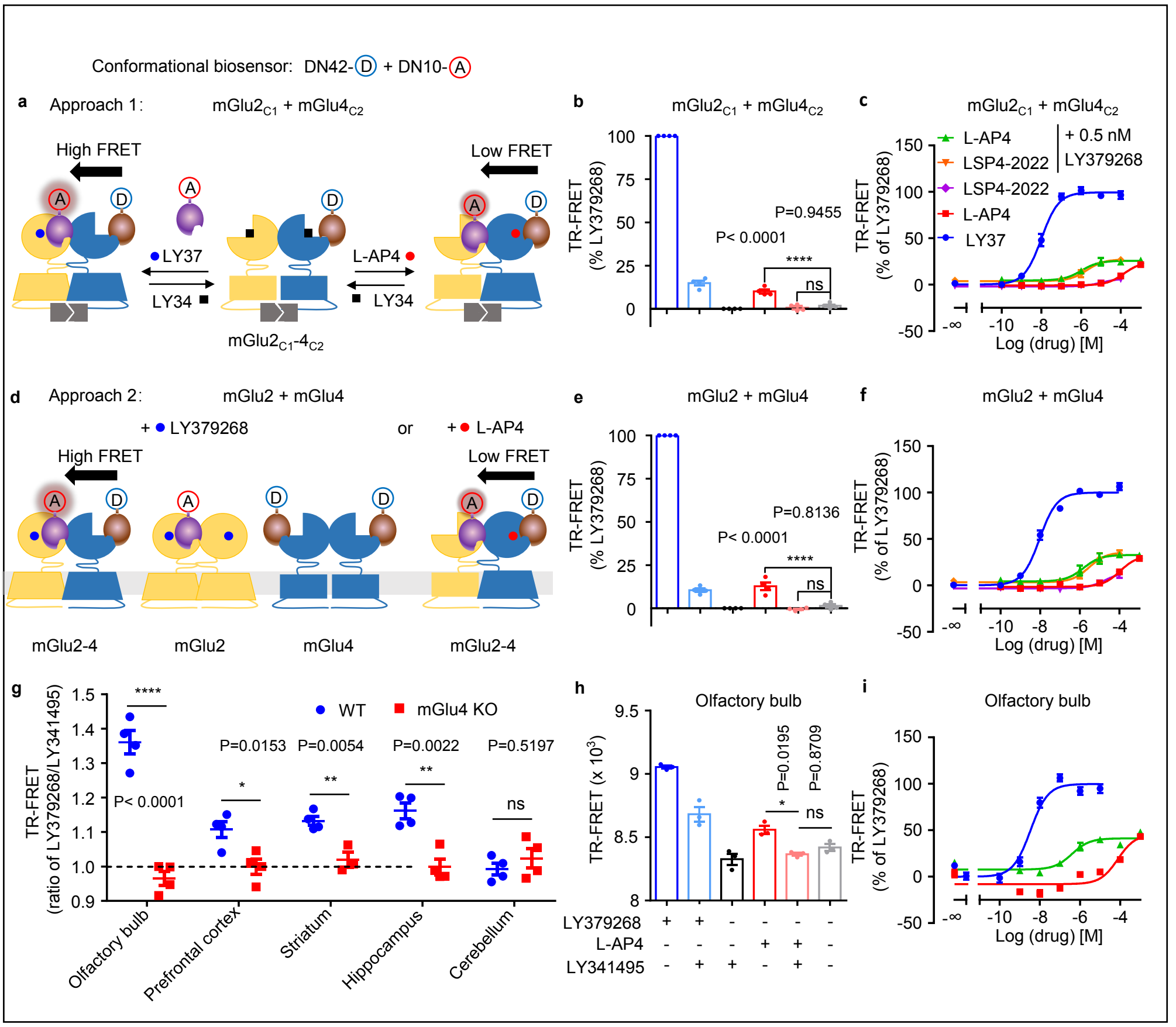
Conformational biosensor: DN42-D + DN10-A
a
Approach 1:
mGlu2C1 + mGlu4C2
High FRET
Low FRET
LY37
LY34
L-AP4
LY34
mGlu2C1-4C2
b
mGlu2C1 + mGlu4C2
TR-FRET (% LY379268)
P=0.9455
P< 0.0001
****
ns
c
mGlu2C1 + mGlu4C2
TR-FRET (% of LY379268)
L-AP4
LSP4-2022
LSP4-2022
L-AP4
LY37
+ 0.5 nM LY379268
Log (drug) [M]
d
Approach 2:
mGlu2 + mGlu4
+ LY379268
or
+ L-AP4
High FRET
Low FRET
mGlu2-4
mGlu2
mGlu4
mGlu2-4
e
mGlu2 + mGlu4
TR-FRET (% LY379268)
P=0.8136
P< 0.0001
****
ns
f
mGlu2 + mGlu4
TR-FRET (% of LY379268)
Log (drug) [M]
g
TR-FRET (ratio of LY379268/LY341495)
WT
mGlu4 KO
****
P< 0.0001
P=0.0153
*
P=0.0054
**
P=0.0022
**
P=0.5197
ns
Olfactory bulb
Prefrontal cortex
Striatum
Hippocampus
Cerebellum
h
Olfactory bulb
TR-FRET (x 10³)
P=0.0195
*
P=0.8709
ns
LY379268
L-AP4
LY341495
i
Olfactory bulb
TR-FRET (% of LY379268)
Log (drug) [M]

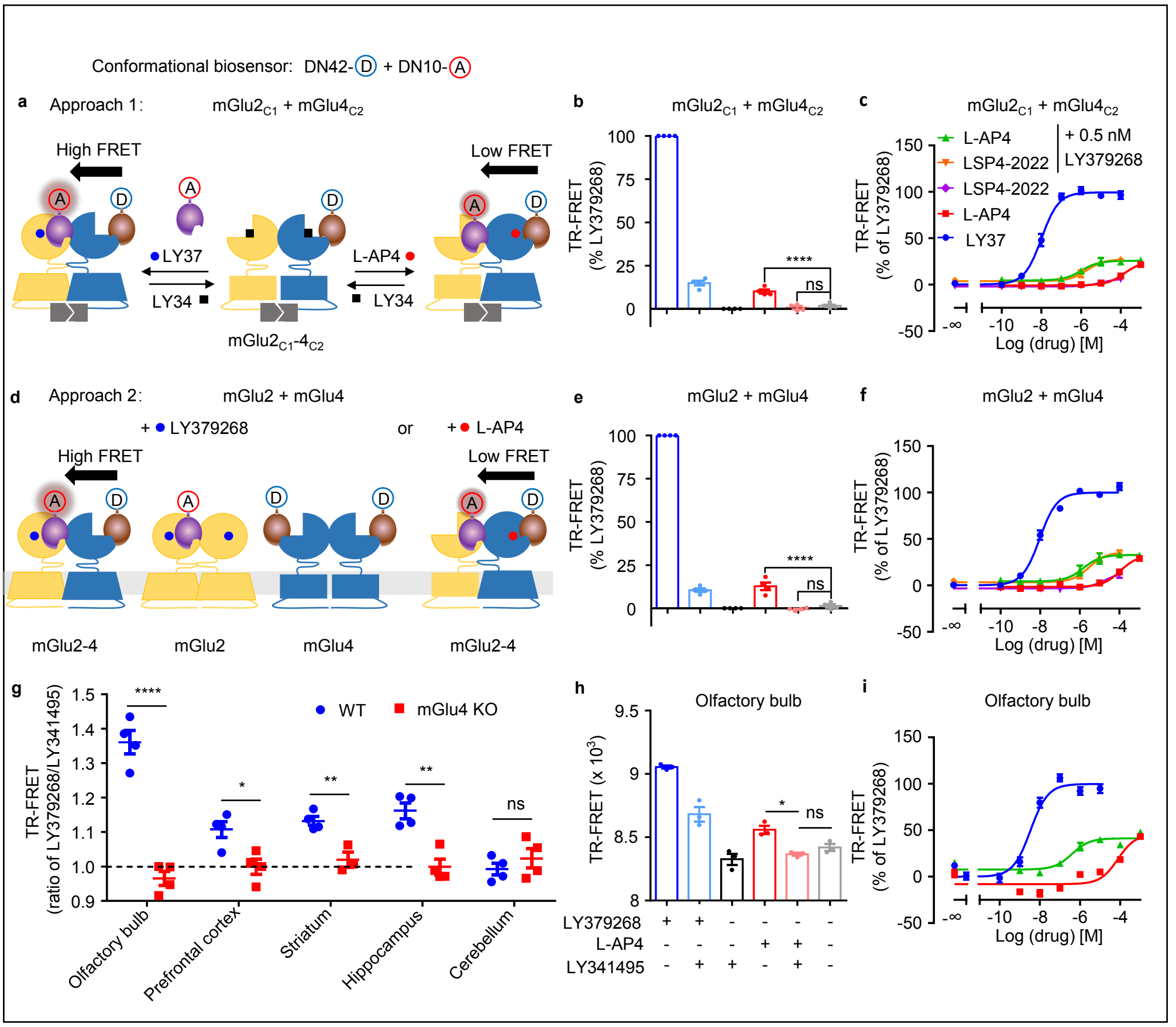
Conformational biosensor: DN42-D + DN10-A
a
Approach 1:
mGlu2C1 + mGlu4C2
High FRET
Low FRET
LY37
LY34
L-AP4
LY34
mGlu2C1-4C2
b
mGlu2C1 + mGlu4C2
TR-FRET (% LY379268)
****
ns
c
mGlu2C1 + mGlu4C2
+ 0.5 nM LY379268
L-AP4
LSP4-2022
LSP4-2022
L-AP4
LY37
TR-FRET (% of LY379268)
Log (drug) [M]
d
Approach 2:
mGlu2 + mGlu4
+ LY379268
or
+ L-AP4
High FRET
Low FRET
mGlu2-4
mGlu2
mGlu4
mGlu2-4
e
mGlu2 + mGlu4
TR-FRET (% LY379268)
****
ns
f
mGlu2 + mGlu4
TR-FRET (% of LY379268)
Log (drug) [M]
g
TR-FRET (ratio of LY379268/LY341495)
WT
mGlu4 KO
****
*
**
**
ns
Olfactory bulb
Prefrontal cortex
Striatum
Hippocampus
Cerebellum
h
Olfactory bulb
TR-FRET (x 10³)
*
ns
LY379268
L-AP4
LY341495
i
Olfactory bulb
TR-FRET (% of LY379268)
Log (drug) [M]

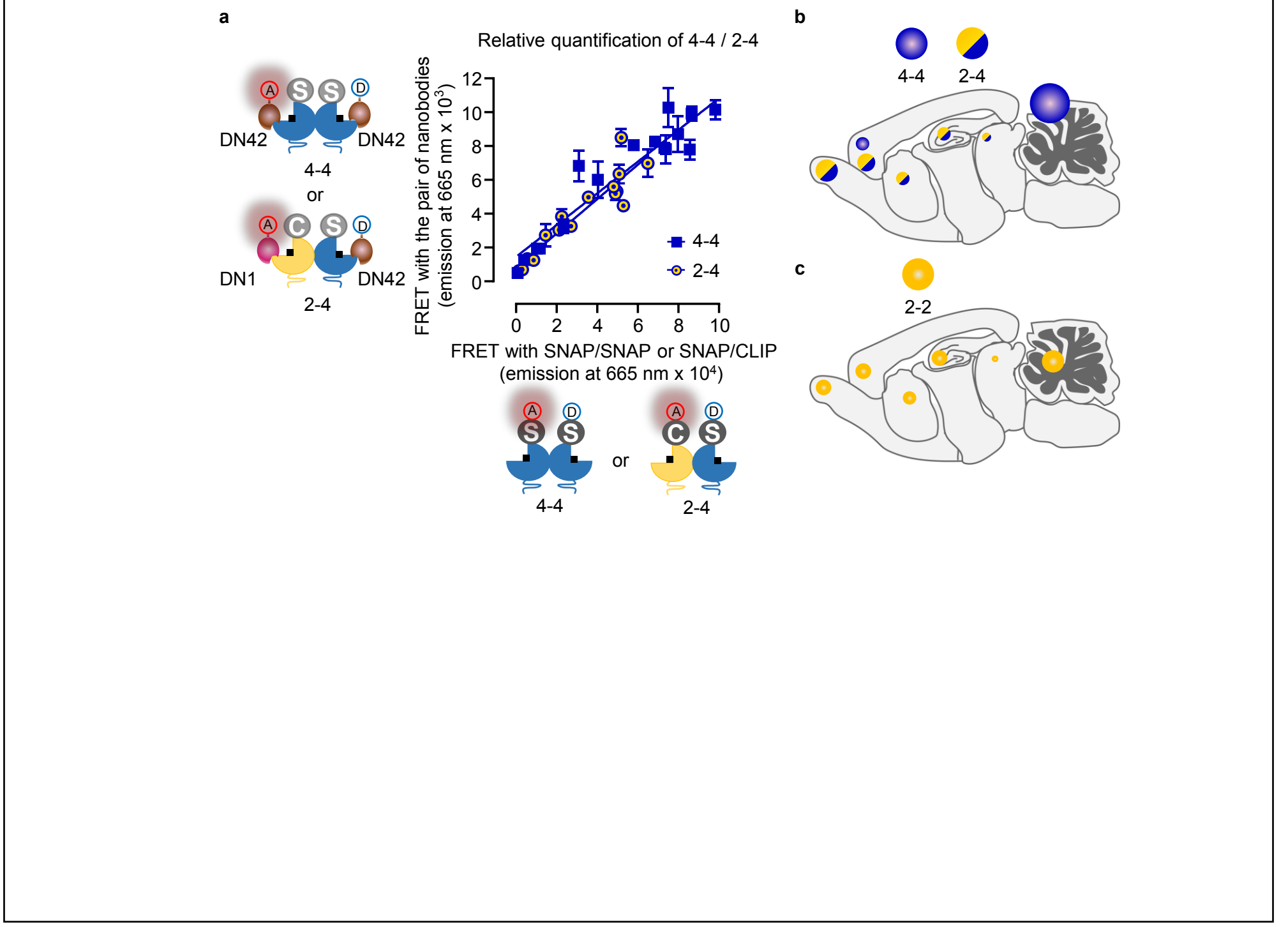
a
Relative quantification of 4-4 / 2-4
A
S
S
D
DN42
DN42
4-4
or
A
C
S
D
DN1
DN42
2-4
FRET with the pair of nanobodies (emission at 665 nm x 10³)
12
10
8
6
4
2
0
0
2
4
6
8
10
4-4
2-4
FRET with SNAP/SNAP or SNAP/CLIP (emission at 665 nm x 10⁴)
A
D
S
S
4-4
or
A
D
C
S
2-4
b
4-4
2-4
c
2-2